2011

BENCH-SCALE, MULTIFILAMENT SPINNING CONDITIONS EFFECT ON THE STRUCTURE AND PROPERTIES OF POLYACRYLONITRILE PRECURSOR FIBER

Elizabeth Ashley Morris
University of Kentucky, ashley.morris@uky.edu

ABSTRACT OF THESIS

BENCH-SCALE, MULTIFILAMENT SPINNING CONDITIONS EFFECT ON THE STRUCTURE AND PROPERTIES OF POLYACRYLONITRILE PRECURSOR FIBER

Due to its unique characteristics, carbon fiber is one of the leading materials for light weight, high strength and stiffness applications in composite materials. The development of carbon fibers approaching theoretical strengths and stiffness is a continuing process which has led to improved mechanical and physical properties over the recent years. Improvements in carbon fiber properties are directly dependent on the quality of the precursor fiber. Research and development of PAN precursor fiber requires extensive experimentation to determine how processing conditions affect the structure and properties of the precursor fibers. Therefore, it is the goal of this thesis to analyze the results of varying coagulation rates on fiber shape, density and porosity, to determine the effect of cross-sectional shape, density, and fiber diameter on the tensile strength of the fiber, and to investigate the most effective method for the reduction of fiber diameter. Results indicate a low temperature, high solvent concentration coagulating bath leads to a rounder cross section with lower void content. Reduction in fiber diameter was found to increase tensile strength while increased molecular orientation experienced during high draw down ratios led to an increase in fiber modulus.

KEYWORDS: Carbon Materials, Carbon Fiber, Precursor, Polyacrylonitrile, Wet Spinning

Elizabeth Ashley Morris

May 6, 2011

BENCH-SCALE, MULTIFILAMENT SPINNING CONDITIONS EFFECT ON THE STRUCTURE AND PROPERTIES OF POLYACRYLONITRILE PRECURSOR FIBER

By

Elizabeth Ashley Morris

Rodney J. Andrews, Ph.D.

Director of Thesis

James M. McDonough, Ph.D.

Director of Graduate Studies

April 5, 2011

RULES FOR THE USE OF THESES

Unpublished theses submitted for the Master's degree and deposited in the University of Kentucky Library are as a rule open for inspection, but are to be used only with due regard to the rights of the authors. Bibliographical references may be noted, but quotations or summaries of parts may be published only with the permission of the author, and with the usual
scholarly acknowledgments.

Extensive copying or publication of the thesis in whole or in part also requires the consent of the Dean of the Graduate School of the University of Kentucky.

A library that borrows this thesis for use by its patrons is expected to secure the signature of each user.

Name	Date

THESIS

Elizabeth Ashley Morris

The Graduate School

University of Kentucky

2011

BENCH-SCALE, MULTIFILAMENT SPINNING CONDITIONS EFFECT ON THE STRUCTURE AND PROPERTIES OF POLYACRYLONITRILE PRECURSOR FIBER

THESIS

A thesis submitted in partial fulfillment of the
requirements for the degree of Master of Science in
Mechanical Engineering in the College of Engineering
at the University of Kentucky

By

Elizabeth Ashley Morris

Lexington, KY

Director: Dr. Rodney Andrews, Professor of Chemical and Materials Engineering

Lexington, KY

2011

For My Mom

Acknowledgements

I would first like to thank my advisor, Dr. Rodney Andrews, for being a constant encouragement and guide throughout my academic career. Without his words of advice, this thesis would not have been possible. I also want to thank Dr. Mark Meier and Dr. Kozo Saito for serving on my examining committee. I am very thankful for the devotion of their time and effort toward the discussion of my thesis.

I would also like to thank Dr. Matthew Weisenberger for being a constant mentor in this field. His experience and dedication has been an inspiration to me in my own research. His technical support and advice throughout the years has led me to the completion of this thesis.

I want to thank the staff of the University of Kentucky Center for Applied Energy Research and especially the Carbon Materials group. I give special thanks to my colleagues in the Carbon Materials group, including Terry Rantell, John Craddock, Mark Taylor, Keith Etheredge, and Dali Qian.

Finally, I would like to thank my family and friends. My husband, Jad, has been a constant encouragement to me in all that I do. My mother, who has always believed in me and taught me the value of hard work and devotion and my brother and sister, who continue to be an inspiration to me. My friends and family have made me the person I am today and I am eternally grateful for their support and encouragement.

TABLE OF CONTENTS

List of Tables

List of Figures

1 Introduction

Due to its unique characteristics, carbon fiber is one of the leading materials for light weight, high strength and stiffness applications in composite materials [1, 2]. The development of carbon fibers approaching theoretical strengths and stiffness is a continuing process which has led to improved mechanical and physical properties over the recent years. Improvements in carbon fiber properties are directly dependent on the quality of the precursor fiber [1, 3-5], which is often prepared using polyacrylonitrile (PAN), rayon, and pitch, among other polymers. However, PAN-based carbon fibers dominate the market due to their good strength and modulus properties [6]. High quality PAN precursor fiber is known to have fewer voids, smaller diameter (approximately 10-12 μm in diameter), low comonomer content, carbon yield higher than 50% and high modulus and tensile strength [2, 5, 7, 8] .

Research and development of PAN precursor fiber requires extensive experimentation to determine how processing conditions affect the structure and properties of the precursor fibers. The development of high strength, high modulus precursor fiber is not a simple task, but involves the cooperation of hundreds of dependent and independent variables, each of which impacts the resultant fiber. As a result, in-depth analysis and understanding of the spinning process and its effect on the resultant fiber is necessary. The factors being studied in this thesis were chosen based on their impact on the tensile strength and modulus of the fiber. Therefore, the factors chosen for analysis include the spinning dope composition, spin bath composition, and spin bath temperature. The goal of this thesis is to study these processing conditions and determine the appropriate conditions for producing a fiber with high tensile strength and modulus. The following is a review of the recent developments in the production of high quality PAN precursors.

1.1.1 Solvent and Polymer Selection

The spinning process is largely influenced by the characteristics of the polymer solution, also known as the spinning dope. Spinning dopes are produced using various organic and other solvents. Solvents used to make spinning dopes often have polar molecules with large dipole moments and low molecular weights. Some of the most common solvents

used include dimethylformamide (DMF), dimethylacetamide (DMAc), and dimethylsulfoxide (DMSO) [9]. Dimethylformamide and dimethylacetamide tend to be the most commonly used solvents in commercial production, each occupying approximately 24% of production capacity. Solvent choice can impact the characteristic fiber structure. Each solvent has its own set of coagulation variables and polymer concentration factors which must be optimized in the spinning process.

Determining the type and concentration of polymer is essential to producing a spinnable dope and ultimately a high-performance carbon fiber. Polymers for use in developing high-performance carbon fiber should have a high molecular weight (~10^5), appropriate molecular weight distribution, and minimal molecular defects [8]. For wet spinning, the polymer weight average molecular weight is typically 100,000-120,000 and solution viscosities range from 50-60 Pascal-seconds. Polymer concentration varies depending on solvent type. Typical examples include DMF, which typically contains 28-32% polymer, while DMAc typically contains 22-27% polymer. All of these numbers are subject to design considerations of the spinning system and spinnerette, as will be seen shortly. However, lowering the polymer concentration can cause significant changes to the fiber structure [3, 8]. For example, Tsai found that higher polymer concentrations led to more circular cross-section fibers, which will be discussed later, but is important to the mechanical properties of the fiber [10].

As stated previously, polyacrylonitrile (PAN) polymer is a typical and common selection for spinning acrylic fibers due to its high carbon yield. A.K. Gupta reviewed PAN precursors for carbon fibers and found that among them, PAN has a high carbon yield and is capable of tailoring with various comonomers for improvements in final fiber properties. PAN homopolymer use as a precursor polymer leads to poorer quality carbon fiber as opposed to a copolymer of PAN with a low percentage of comonomer [8]. Drawability of homopolymer PAN is limited due to the hydrogen bonds of the structure [2]. These same bonds also cause the PAN homopolymer to gel very quickly, but the addition of comonomers lowers the gelation rate, making the spinning dope easier to work with [5]. Common comonomers include vinyl comonomers with acidic groups like acrylic acid, methacrylic acid, and itaconic acid. Among these comonomers, itaconic

acid appears to be superior, due to the presence of two carboxylic groups, which increases the possibility of interaction between carboxylic groups and adjacent nitrile groups. Also important is the amount of comonomer to be used. The proportion of comonomer used has a direct impact in the processes of stabilization and carbonization and the final carbon fiber properties. For itaconic acid, it was found that an increase in the comonomer content reduces the time required for thermooxidative stabilization and improves mechanical properties, but reduces the carbon yield. Results have shown about 2 mol % to be the ideal content for acidic comonomers. Any higher leads to poor yield in carbon fibers [8].

1.1.2 Dry and Wet Spinning Processes

Solution spinning of polyacrylonitrile into fiber is typically done in one of two ways: dry spinning or wet-spinning. Dry spinning involves pumping the polymer solution (dope) through a spinnerette and into a tower with a flow of heated inert gas, causing the solvent in the dope to vaporize and the fiber to solidify. Wet-spinning involves the extrusion of the dope through the spinnerette and into a bath containing a coagulant, usually a mixture of solvent and non-solvent, such as water. The fiber then proceeds through a coagulation bath, coagulating the fiber slowly until it forms a dense structure. This coagulation occurs due to solvent diffusing out of the polymer solution and non-solvent diffusing into the forming fiber [3, 8, 9]. The cross section of precursor fibers is fixed when leaving the coagulation bath [4]. There is a variation of wet-spinning known as dry jet wet-spinning in which the spinnerette is not in contact with the coagulant during spinning, but rather the spinning solution leaves the spinnerette and travels through a small air gap before entering the coagulation bath. Standard wet-spinning accounts for 85% of the production of acrylic fiber around the world [3] and allows for wide variations in the fiber properties due to the variation in spinning parameters, such as the spinnerette capillary diameter, the throughput rate, and take up velocity. Stretching during spinning and the coagulation conditions also influence the molecular orientation and subsequent modulus and strength of the fiber [8].

1.1.3 Coagulation Mechanism

Coagulation is an important step in the formation of solution-spun filaments. It is influenced by polymer composition, coagulation bath composition, coagulation bath temperature and spin draw, which is defined as the ratio of the first roller take-up velocity to the dope extrusion velocity [5]. Coagulation of the fiber depends on two diffusion processes. One process transports solvent out of the filament and into the bath and the other transports non-solvent from the bath into the fiber. Both happen simultaneously. The balance of these two process leads to precipitation of the polymer into fibrillar form [11]. The composition and temperature of the coagulation bath determine the rate of coagulation, with higher concentrations of the non-solvent, and higher temperature leading to high coagulation rates. However, lower rates of coagulation are preferred, because as coagulation is slowed, more time is allowed for the internal adjustment of osmotic stresses resulting in a denser fiber and less skin formation [12]. Coagulation is slowed by spinning into a low temperature bath with high solvent content, resulting in the fluid entering the gel state [8], with gelation being defined as the transition of the polymer from liquid phase to gel when temperature, concentration of the precipitant, and mechanical stress change. Gelled fibers are often stretched for better orientation and mechanical properties. Increasing orientation during the gel state is aided by the trapped solvent within the fiber that decreases the cohesive forces among the nitrile groups of the polymer chains [8]. Orientation is vital to the development of fiber with high tensile strengths and will be discussed later. It can therefore be concluded that spinning into a low temperature bath is fundamental to development of high strength fiber.

In order to determine the rate at which coagulation is occurring, it is important to monitor the concentration of solvent within the fiber at varying points along the spinning line. Therefore, the amount of solvent remaining in the fiber, or residual solvent, is calculated to give such an indication. Cheon determined the concentration of solvent in filaments by removing fiber from the bath and removing excess moisture and then placing the filament in a specified amount of water for a time sufficient to extract the solvent from the filament. The spinning solvent used was nitric acid; therefore the solvent concentration was measured using NaOH titration.

He found that the diffusion rate increases as the solvent concentration of the coagulation bath decreases [13]. Similarly, Chen determined the concentration of residual solvent by extracting into water. The solvent concentration in the water was measured by $KMnO_4$ back titration method.

The DMSO residual content by percentage was compared to residence time within the coagulation bath [2] and showed a sharp decrease in DMSO concentration in the fiber within the first few seconds, which gradually begins to slow as the concentration gradients change and begin to reach equilibrium.

1.2 Precursor Fiber Structure

1.2.1 Skin-Core Structure

Coagulation is important to the final fiber properties as it determines the structure of the fiber [14-16]. This structure, depending on the rate of coagulation, results in what is often referred to as a skin-core structure. This skin-core structure is explained by Heyi Ge, and also by Chen, as a multilayer structure [5, 11]. The outer layer is known as the skin and is a white, dense layer, which is followed by the cortex, endothecium, and finally the core, as seen in Figure 1.1 below. From skin to core, each thickness was determined to be 0.2-0.3 μm, 2-3 μm, 2-3 μm, and 6-7 μm, respectively.

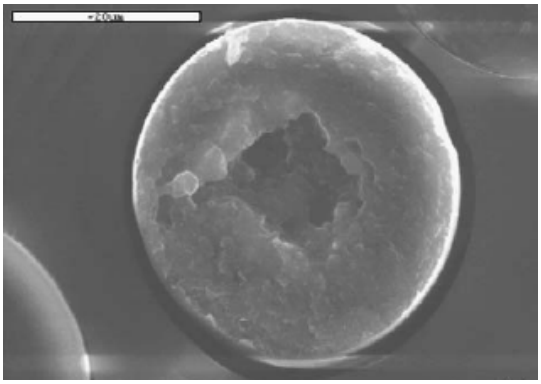

Figure 1.1. Skin core structure of nascent fiber

(With kind permission from Springer Science+Business Media: Journal of Polymer Research, Study on the Coagulation Mechanism of Wet-Spinning PAN Fibers, 13, 2006, 518, Juan Chen et al, Figure 9, Springer 2006.) [11]

This stacked layer structure, as shown in Figure 1.2, allows for varying levels of diffusion throughout the fiber. While the skin is composed of stacked, sheet like layers, the core is loose, leading to voids which are detrimental to fiber strength. Heyi Ge and Chen found that solvent concentration in the outside layers (0.2R, where R is fiber radius) decreases rapidly forming a dense layer in a short time, as was found in the residual solvent calculation by Chen, and drops slowly in inner layers (0.8R) [7, 11, 17] .

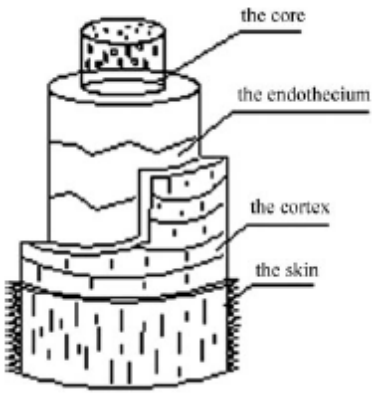

Figure 1.2. Structural model of PAN precursor fiber (Figure from Heyi Ge et al) [17]

The dense outer layer is composed of randomly oriented fibrils, which Bell found to become oriented through stretching in the coagulation bath [16, 18]. Shear fields at the spinnerette capillary exit also orient the PAN structure parallel to the direction of flow [5]. Peng performed an experiment spinning fibers at various dope extrusion velocities ranging from 0.43 to 7.32 m/min and therefore at different levels of shear, ranging from 409.5 s^{-1} and 6971.4 s^{-1}, apparent shear rates, respectively. He found that with increasing dope extrusion rates, the skin core structure was more obvious, suggesting that with the increase in dope extrusion rate, the jet swell became larger, with the surface more oriented by the shearing. The jet swell also resulted in hindering diffusion, causing insufficient coagulation of the inner part [4]. Therefore, while orientation does occur through the spinnerette capillary, further stretching is required to fully orient the structure during coagulation. Knudsen found that stretching of the fiber in boiling water orients the fiber in the direction of the fiber axis and also stretches the individual fibrils [15]. Further, Moreton performed an experiment varying the amount of fiber stretching done in

a steam tube at 100 °C. Prior to entering the steam tube, the fiber passed through a wash bath at 50 °C before passing through the 45 cm steam tube. He found the optimal steam stretch ratio to be up to x 13. At higher ratios, the fiber tends to break. He does state, however, that increased breakages may have occurred due to the spinning solution being filtered only to 20-30 μm [18]. Filtration of dope helps in the improvements of final fiber properties as well as fiber spinning stability [8] and is therefore necessary for maximum stretch ratios. Again, this higher stretch leads to higher orientation, lower elongation, and a higher fiber modulus [12]. Lower coagulation temperature is preferred because network density increases as coagulation temperature decreases, leading to shorter, densely packed fibrils [16] and, if obtained in the gel state, the skin-core structure and the pore density at the surface can be decreased [8, 12].

1.2.2 Void Development

As stated previously, a loose core leads to increased voids within the fiber. This loose core is characterized by a fibrillar, open, and unoriented structure. Wet-spun fibers are known to have a loose core, with voids about 0.02 μm in diameter [14, 15]. Knudsen found that the pore radius was higher for fiber spun in an organic solvent at a high spin bath temperature when compared to those from a low temperature bath [7, 15], again supporting the use of a low temperature coagulation bath. Bell also found that at higher coagulation temperatures, macroscopic voids within the fiber increased [16]. The model by F.R. Barnet seen in Figure 1.3 represents fiber spun in spin baths at low concentrations, high temperatures and high draw rates [14]. He found that acrylic fibers have a circumferentially oriented crystalline structure surrounding a radially oriented interior which often contains elongated voids with widths of 1-4 μm, distributed at an average concentration of 80 mm^{-1}. He describes the microstructure as capillaries arranged radially in the filament cross sections [14].

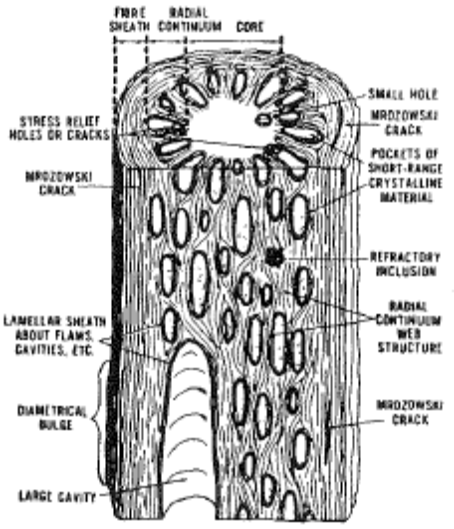

Figure 1.3. Structural model for high-modulus fiber

(Reprinted from Composites, F.R. Barnet and M.K. Norr, A Three-Dimensional Structural Model for a High Modulus PAN-Based Carbon Fibre, 93-99, Copyright (1976), with permission from Elsevier) [14]

In determining the source of these voids, Knudsen found their formation to be due to penetration of the coagulation bath into the fiber through surface faults, which would explain the uniform presence of many voids. Once the dense outer layer is penetrated, the loose core is susceptible to void formation. This rupturing of the fiber surface during coagulation comes as the stress from stretching increases [12, 15, 19] and can be seen in Figure 1.4 [15]. Figure 1.4 shows a longitudinal, unoriented, uncollapsed view of a precursor fiber with uniform voids present.

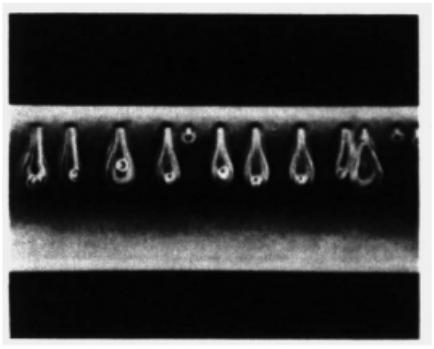

Figure 1.4. Uniform voids within precursor fiber (Figure from Craig et al) [15]

In order to study the void formation of precursor fiber, the porous structure of the gel fiber is preserved by freeze drying. If not preserved, the structure of the fiber will collapse as the fiber dries and much of the original porosity will be lost [7, 12]. Knudsen found that such freeze drying was indeed necessary due to the repeatability of results in surface areas and densities compared to values obtained on samples dried at room temperature or elevated temperatures without freeze drying [12]. S.J. Law and Knudsen presented a freeze drying technique which first involved placing the washed samples into liquid nitrogen [7, 12]. Samples were then transferred to a precooled vessel with suitable sublimation rates between -20 °C and -30 °C at a pressure of 10^{-2} to 10^{-3} mbar. The total removal of water can be checked by allowing the vessel to warm to room temperature and monitoring the pressure. Significant loss of pressure requires further drying of the samples [7].

D.J. Thorne also performed a study of the internal flaws in acrylic fiber. He used optical microscopy to observe the internal flaws of the fibers, which were mounted parallel on microscope slides, immersed in cedar oil, and then viewed in transmitted, polarized light at magnifications of x200 to x2000. The number of internal flaws and distances between them were recorded. Flaws which occurred within 0.1 mm of each other were classified as one flaw. He classified voids by their shape and size. More cylindrical voids were concluded to be caused by gases dissolved in the fiber spinning dope and the irregular voids were more likely to be caused by irregular flow at the spinnerette orifice [20]. Therefore, not only is it important to regulate the stretch the fiber experiences to minimize void formation, but also to properly de-aerate the spinning solution prior to spinning. Other methods for decreasing the occurrence of voids include increasing the dope solids, or weight percent polymer in solvent, which leads to an improvement in the homogeneity of fiber structure [12]. The use of high solids content within the dope can also lead to formation of gels within the dope and difficulty spinning, therefore the benefits and costs must be carefully weighed.

Often the number of voids within the fiber can be described by the fiber density. Numerous methods have been used in the determination of fiber density. Knudsen often performed fiber density measurements using immersion in wetting and non-wetting liquids, and also by internal fiber surface area by gas adsorption [12].

Knudsen found that the density in a wetting liquid decreases with increasing amounts of residual solvent within the fiber. This indicates the existence of non-communicating voids in the fiber [15]. Therefore, fibers with numerous voids have lower densities than a fiber with a tightly packed structure.

1.2.3 Fiber Cross Section

As stated previously, the fiber structure is determined by many variables, the most dominate being the rate of coagulation. Fibers produced by wet spinning tend to have a circular or dog-bone shaped cross-sectional area depending on the rate of coagulation. A circular cross-section is characteristic of wet spun fibers [5]. Tsai found that the shape of the cross-section is one of the most important characteristics of fibers, with deviation from circularity leading to luster, mechanical, and other physical properties being affected [10]. For example, precursor fibers with non-round cross-section cannot withstand a high draw ratio during subsequent spinning, stabilization, and carbonization due to stress concentration [2]. Circular fibers, on the other hand, experience a homogeneous Poisson's contraction when exposed to tensile forces. Achievement of a circular cross section is determined again by the rate of coagulation. It has been found that when the flux of solvent outwards is less than the inward flux, the filament swells and a circular cross-section can be expected. This swelling occurs at high bath temperatures and higher solvent content in the coagulating bath [10]. For this reason, cross sections are characteristically round at 50 °C or above. In contrast, at lower coagulation temperatures, the outward diffusion of solvent predominates resulting in non-round sections, higher fiber density [2, 12], and a reduction in diameter [5]. Therefore, the processes for producing circular fibers or high density fibers are competing and it is important to determine whether cross sectional shape, fiber density, or diameter play greater roles in the strength of the resultant fiber.

1.2.4 Fiber Diameter

As stated previously, vital to the development of high strength precursor PAN fiber is the development of a small diameter fiber. With decreases in filament diameters, there has been shown to be a corresponding increase in strength [6]. This can be explained using the Griffith fracture theory, which states that a single molecular chain would possess the highest strength because such a structure could tolerate no defects [21], ultimately resulting in fewer defects per unit length. Reducing the filament diameter by stretching also improves the orientation of the molecular chains, increasing modulus, and limits the formation of a skin-core, as a smaller diameter allows for even diffusion. One way to improve stretch ratio is to stretch through hot water or steam, as PAN has a glass transition at approximately 100 °C and becomes quite plastic at 180 °C. Stretching can be achieved by stretching through ethylene glycol at 140 °C and glycerol at 180 °C [6]. Other options include reducing the dope extrusion rate. For example, with increasing dope extrusion rate, the average diameter of the nascent fiber increased due to the increased jet swell and the surfaces of the fibers were rougher compared to lower extrusion rates [4]. So, it can be concluded that in order to reduce diameter, stretching through steam or glycerol is necessary, along with reducing the dope extrusion rate.

1.3 Rheology

Understanding the rheology of the spinning dope is vital to optimizing the spinning conditions and resulting precursor fiber. Rheology of the spinning dope serves as a quantitative analysis of the dope properties, which in turn gives information about the "spinnability" of the dope. Several studies have been done to provide an adequate rheological process to simulate the effects of spinning the solution through a spinnerette plate and into the coagulating medium, therefore defining spinning viscosity, or "spinnability." Petrie found that defining dope spinnability was not a simple task, but was complicated by controllability of the spinning flow, flow history, extrudate swell, and rate of strain [22].

1.3.1 Shear Viscosity

Shear viscosity can give a general idea of the dope properties. For example, Ferguson investigated a series of solutions at various PAN concentrations and at different water contents. The shear flow rates are shown in Figure 1.5 [23].

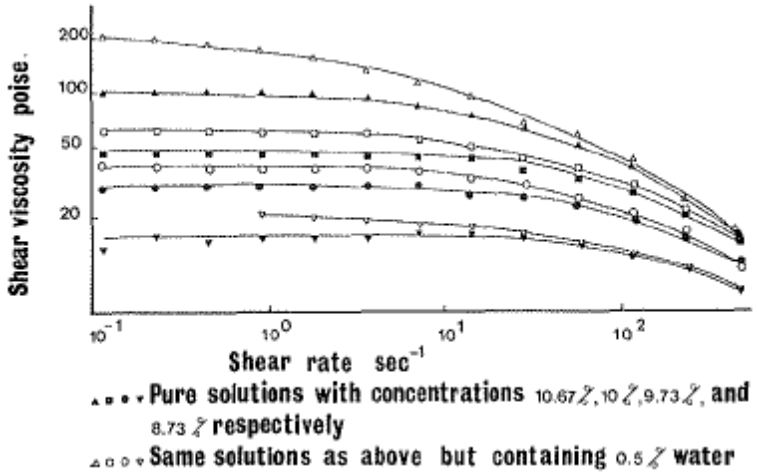

Figure 1.5. Shear viscosity versus shear rate

(Reprinted from Journal of Non-Newtonian Fluid Mechanics, J. Ferguson, Rheological and Coagulation Features in the Wet Spinning Process, 333-338, Copyright (1980), with permission from Elsevier) [23]

He found the solutions to be Newtonian at low shear rates, becoming non-Newtonian above 10 s^{-1}. Under shear flow, polymer molecules tend to align in the direction of flow [5], therefore the relaxation would be slowed as water diffuses into the polymer solution. When water was added to the solution, the reduction in solvent power of the DMF encouraged chain coiling, while elongational forces stretched the molecules. The behavior of the solution depended on which was dominant. Reduction in elastic modulus was found to be caused by coiling of the macromolecules as solvent power decreases with increasing water content [23]. From this experiment, it is clear that the addition of water to the dope increases the shear viscosity. While shear viscosity data is relevant, modeling of the spinning process and filament formation has been done using extensional rheology, in which a normal tensile force (as in real fiber spinning) is applied to the polymer solutions.

1.3.2 Extensional Rheology

Extensional viscosity is valuable for quantifying the spinning process. Compared to shear viscosity, extensional viscosity can have values for resistance to flow orders of magnitude higher. The first filament stretching devices used a small cylindrical mass accelerating freely under gravity to stretch a small liquid bridge connecting the mass to a stationary transport. Photographic analysis was then used to determine the rate of decrease in the radius of the filament under constant force. This basic technique has since been upgraded to enhance the understanding of the fluid mechanics of filament stretching, the physics of dilute polymer solutions in strong extensional flows and the dynamics of extensional flow instabilities that have so far been described as the fluid "spinnability" [24].

Sridhar determined the extensional viscosity of a fluid consisting of 0.185 wt.% polyisobutylene in a solvent of kerosene and polybutene by placing a sample of the fluid between two Teflon discs, with the bottom disc being attached to the central shaft of an MTS material testing machine. The fluid was stretched in air at a constant overall stretch rate, k, of 0.3 s^{-1} . It was apparent from his experiment that two stretching regions formed. The local extension rate, $\dot{\epsilon}_1$, based on filament diameter was significantly greater than the overall stretch rate. The initial high stretch rate region relates directly to the necking of the fluid column caused by sudden stretching from the rest state. This non-uniform stretching lasts approximately half the time it takes the fluid to reach the maximum stable length. He found the dependence on the initial dimensions of the fluid sample to be irrelevant to the viscosity measurements. The deformation was found to be uniform, and independently imposed, and the total strain measurable [25]. This is one example of the use of extensional viscosity to simulate spinning conditions and to determine the spinnability of certain dopes. However, the use of extensional viscosity measurements to quantify the spinning process is limited. For example, in wet spinning, the ratios of polymer to solvent to coagulant changes rapidly, but during extensional viscosity measurements, the solution conditions remain constant.

1.4 Spinnability

1.4.1 Modeling Spinnability

In order to develop a stable spinning process and have the ability to modify that process to fit the end needs, it is important to understand the spinnability of a given spinning solution. That is, the ability of the solution to form fiber under tension. Fiber spinnability is affected by numerous variables, including rheological properties of the spinning solution, spin draw, capillary size and shape, and rate of mass and heat transfer between the extruded filament and the coagulation bath [26].

In modeling fiber spinnability, the hydrodynamic force is often compared to the tension force acting on a fiber, along with the fiber drag being compared to the fluid inertia. Ockendon referred to these ratios as α and β, respectively. He presented the derivation of a model based on these ratios when applied to the spin bath of the process, where he stated that $\alpha \ll 1$ and $\beta \gg 1$, meaning that the tension is much greater than the hydrodynamic force in the spinning bath and that the fluid drag was much greater than the fluid inertia. He also assumed steady flows, and a large number of filaments within the tow, which allows variations in fluid velocity and pressure on a length-scale compared with radius to be neglected. He found that the equations for fluid flow on the macroscopic scale are equivalent to those for flow in an anisotropic porous medium, such as the flow through a sintered metal filter element. When compared to experimental results, the model showed good qualitative agreement [27].

Similarly, C.D. Han performed a study on fiber spinnability in which he studied the theoretical aspect of spinnability in the absence of change of temperature and composition and focused mainly on the force balance equation for a steady liquid jet under uni-axial tension. He also stated that force exerted from fiber drag is much greater than the fluid inertia and presented the following force balance equation [26].

$$F_{ext} = F_{rheo} + F_{drag}$$

Where F_{ext} is the external tensile force exerted by the take-up device and has the value F_L. F_{rheo} is the rheological force which is connected with the deformation of the liquid thread and it varies along the spinning way and F_{drag} is the frictional force exerted by the

surrounding medium on the continuously stretching liquid thread. These variables are all important to the development of a stable spinning process [26].

One important study by Mewis points out that a viscoelastic fluid has a memory of its mechanical history, and therefore the shear in the spinnerette capillaries and the feed system can affect the behavior on the spinning line, but found that nonlinear generalized Maxwell models can accurately describe the detailed behavior under spinning. Therefore it is important to consider that factors that may be thought of as dominant forces for viscoelastic fluids in general may be altered in the experimental sense [28].

1.5 Conclusions

In conclusion, it was found that for the spinning of high-quality PAN precursor, several variables must be analyzed. First, the selection of a polymer. It has been shown that PAN homopolymer use as a precursor polymer leads to poorer quality carbon fiber as opposed to a copolymer of PAN with a low percentage of comonomer [8]. The coagulation process must also be monitored to ensure optimum coagulation conditions. It was shown that orientation is vital to the development of fiber with high tensile strengths and was concluded that spinning into a low temperature bath is fundamental to development of high strength fiber. When considering the structure of the resultant fiber, again, slower coagulation is preferred because network density increases as coagulation temperature decreases, leading to shorter, densely packed fibrils [16]] and, if obtained in the gel state, the skin-core structure and the pore density at the surface can be decreased [8, 12]. As far as cross-sectional shape is concerned, it is widely known that circular fibers experience a uniform Poisson's contraction when exposed to uni-axial forces and are therefore capable of handling high tension forces. It has been found that cross sections are characteristically round at 50 °C or above but that in contrast, at lower coagulation temperatures, the outward diffusion of solvent predominates resulting in non-round sections, higher fiber density [2, 12], and a reduction in diameter [5]. Therefore, it is important to determine whether cross sectional shape, fiber density, or diameter play greater roles in the strength of the resultant fiber. This strength has also been found to be affected by decreases in filament diameters [6] which is explained using the Griffith fracture theory, which states that a single molecular chain would possess the highest

strength because such a structure could tolerate no defects [21]. Reduction in diameter can be achieved in many ways, from stretching in glycerol or steam, or reducing the volumetric flow rate of dope through the spinnerette, all of which must be investigated to determine the most effective method. Rheology must also be carried out in order to quantify desirable properties in a spinning dope.

Therefore, it is the goal of this thesis to analyze the results of varying coagulation rates on fiber shape, density and porosity, to determine whether cross-sectional shape, density, or fiber diameter play a greater role in the tensile strength of the fiber, and to investigate the most effective method for the reduction of fiber diameter.

2 Bench-Scale PAN Precursor Fiber Spinning Line

2.1 Introduction

Effective, scale-able research and development of experimental precursor fiber requires bench scale spin line characteristics similar to industrial production. The development of such a line is an evolving process, utilizing results gathered from successive spinning attempts, and those in the literature. The spin line developed for the purpose of this project employs characteristics similar to small tow industrial lines, but scaled down approximately by several orders of magnitude. This bench-scale line, developed in-house, lends itself to rapid customization to meet the R&D goals.

2.2 Bench Scale Spin Line

The line was developed to provide a constant inlet pressure of polymer spinning solution, known as dope, into a metering pump, which then provides a constant volumetric flow rate to the spinnerette where the fibers first emerge. Two pneumatic cylinders provide continuous pressurization of two 200 mL stainless steel syringes into the dope inlet system. A Zenith PEP-II polymer gear pump then operates at 0.16 cc/rev from 4 to 70 rpm (up to 10,000 psi) to provide constant flow of the solution. Filtration is key, and therefore the use of two 90 micron pore size sintered metal in-line filters, on the outlet of each 200 mL syringe, are used to pre-filter the dope before entering the gear pump. The gear pump then provides a constant flow of dope through a second level of filtration, a 40 micron pore size sintered metal filter cup, for the removal of gels and other agglomerates.

At the extruder head, the dope is again filtered through a 10 micron screen pack before flowing through the breaker plate to the spinnerette.

Spinnerettes are designed differently for wet-jet and dry-jet wet spinning. Wet-jet spinning, i.e. spinning directly into the coagulation bath with no air gap, as opposed to dry-jet wet spinning, or spinning with an air gap, accounts for 85% of fiber production around the world, and has advantages such as a wide variety of solvent choices and high production capabilities [3]. However, if spinning is initiated with the spinnerette submerged in the coagulation bath, the fiber will tend to coagulate as it attempts to exit the capillaries, as a result clogging the capillary. Therefore, spinning begins with the spinnerette face just above the coagulant until spinning solution can be seen to exit the die. At this point, the spinnerette face is lowered to the coagulation bath until just immersed and wet-jet spinning begins.

In Figure 2.1, it can be seen that the fiber continues down a sequence of seven coagulation baths, containing a N,N-Dimethylacetamide (DMAc) and deionized H_20 solution to provide gentle coagulation while godets provide the appropriate stretch ratio. The presence of seven coagulating baths mitigates fiber skin formation through slow, gentle coagulation and also allows for experimental flexibility. The line ends with a heated deionized water bath for hot water stretching of the tow, a steam stretch station, and a purpose-built heated godet station, which was designed and built to dry the fiber prior to take-up on the traversing winder. The stainless steel rollers are heated to between 50 and 55 °C and provide just enough heat to dry and not damage the fiber tow. Rolling wet fiber onto the spools using the traversing winder can often lead to damage to the fiber, due to the fact that as the fiber dries on the spool, it contracts and puts undue stress on the fiber.

Figure 2.1. Spinning line showing sequence of coagulation baths

2.3 Die Configuration

A 100 filament, 60 micron die being used for wet-jet spinning was machined from 316 stainless steel. The capillary length was designed to provide a 2:1 length to diameter ratio (120 micron), with a 60° cone entrance angle and a hexagonal hole pattern. For dry-jet wet spinning, an alternative die was designed which incorporated a 10:1 length to diameter ratio to establish stable, laminar flow in the capillary. This 100 filament, 150 micron die was also machined from 316 stainless steel, but provides a circumferential, or concentric "bolt-circle", arrangement of capillaries to provide optimal spacing for prevention of coalescing upon exiting the spinnerette and is also necessary to attain homogeneous pressure drop across each hole. The flow through each capillary must be identical for stable spinning.

2.4 Pump Customization

Frequent fiber breakages at the die led to the analysis of the metering pump extrudate. Inspection revealed the presence of bubbles in the spinning solution, which were causing fibers to break. Possible causes for the presence of these bubbles were: a) entrained air within the spinning dopes, b) entrance of air into the system during syringe attachment, c) system leaks due to damaged parts/improper assembly, d) pump cavitation/isolated pockets of low pressure.

Checking spinning dopes for entrained air involved simply detaching the syringe from the inlet and allowing the dope to flow into a container to check for the visual presence of

bubbles. The presence of bubbles was negligible, although further precautions such as increased dope de-aeration time under vacuum, to be discussed momentarily, were used to ensure a bubble free solution. It was found, however, that the current configuration, allowed for the entrance of a significant air pocket into the system. Non-return valves, to prevent the fluid from the two syringes from pushing against one another, allowed a pocket of air to be formed between the system filled by the first syringe, and the second syringe. Therefore, when the second syringe was pressurized, it pushed a pocket of air into the pump. This problem was remedied by introduced a bleed into the system, shown in Figure 2.2, which allowed air to escape and can then be capped. However, bubbles persisted.

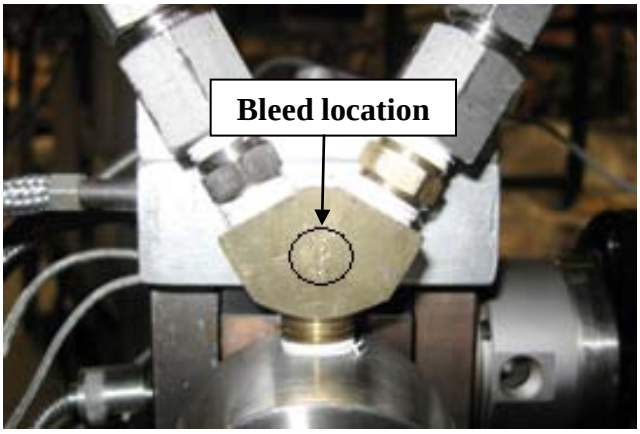

Figure 2.2. Bleed location to remedy air pockets

The presence of two well-defined streams of bubbles in Figure 2.3 led to the belief that it was not in fact a random assortment of bubbles or leakage, but rather an issue with the pump itself. Disassembly showed rounding occurring on the edges of the bearings, as seen in Figure 2.4, suggesting bearings were not always coplanar.

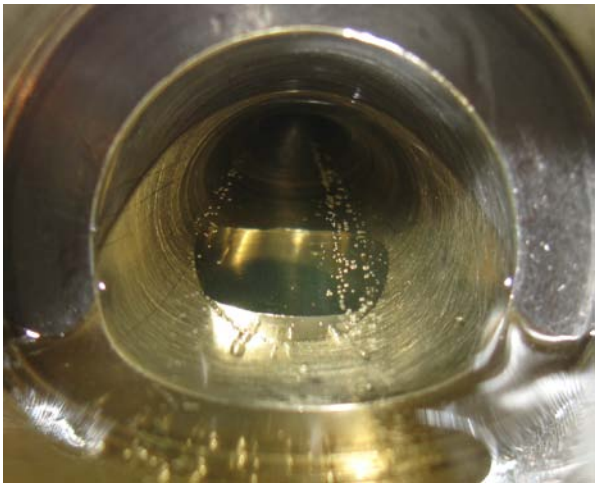

Figure 2.3. Uniform streams of bubbles

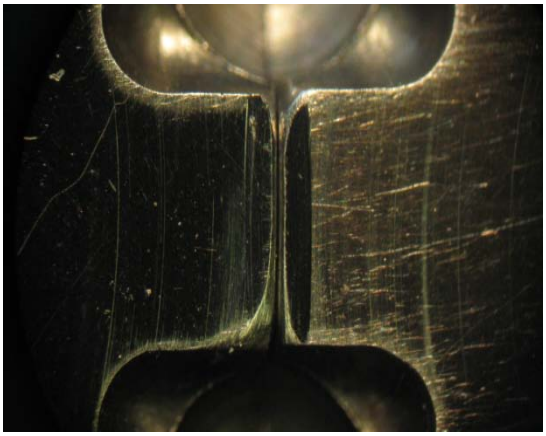

Figure 2.4. Bearings rounded tooth

Upon consultation with the pump manufacturer, this rounding was conjectured to potentially affect metering accuracy but would in fact aid in the introduction of fluid to the gear mesh – a good thing. A series of tests were undertaken to be sure a lack of inlet pressure was not causing a vacuum, or region of low pressure, due to inability of the constant pressure inlet system to "keep up" with the pump. An Omega miniature flush diaphragm pressure transducer was used to measure the inlet pressure of the dope, which was found to be 1800 psi, well above the 300 psi value recommended by pump manufacturer Colfax-Zenith. Due to the tight tolerances of the pump (0.0001 inch), it was hypothesized that the front and rear plates of the pump were blocking the flow of

dope. This bad flow, as explained by Colfax-Zenith, leads to pockets of low pressure during gear mesh. This low pressure then pulls the solvent into a vapor, creating bubbles. This also explained the regularity observed in the bubble streams. To remedy this problem, gaskets were made using 0.001" fluoropolymer, one placed on either side of the pump block to increase side clearance and aid in dope flow, as seen in Figure 2.5.

Figure 2.5. One mil fluoropolymer gaskets to increase side clearance

Figure 2.6. Resulting decrease in bubbles due to addition of gaskets

Attempts to increase the number of gaskets on either side resulted in a slight decrease in bubbles, as seen in Figure 2.6, but a drastic change was required. In order to dramatically change the flow of fluid across the face of the bearings, channels were machined in them, per close consultation of the manufacturer. This was to help introduce fluid into the bearings and prevent pockets of low pressure from forming.

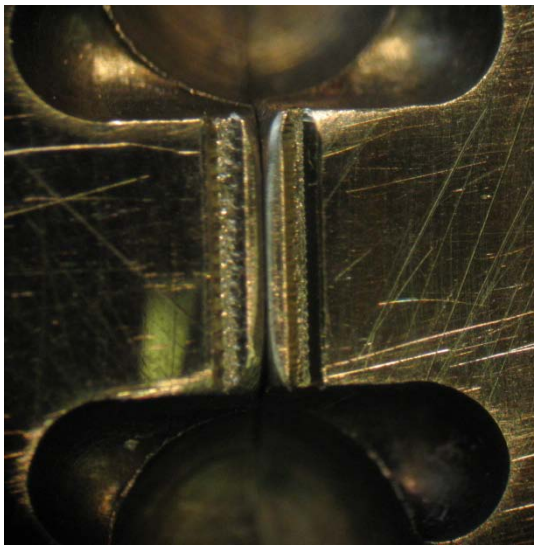

Figure 2.7. Bearings machined with channels

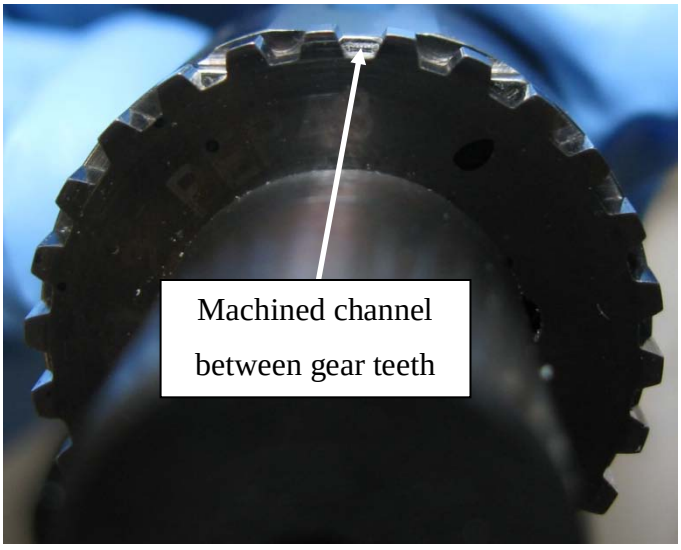

Figure 2.8. Channel between gear teeth

Channels were machined into the bearings as seen in Figure 2.7 and Figure 2.8 in order to introduce the spinning solution to the gears. Along with the use of 4-1 mil gaskets, this led to the near complete removal of bubbles, shown in Figure 2.9, and increased spinning stability at the cost of maximum pump outlet pressure. This, however, was an acceptable trade-off as it solved the more pressing bubble issue.

Figure 2.9. Dope flow without bubbles

2.5 Dope Preparation

2.5.1 Polymer and solvent selection

Dupont found that the solvent selected for the production of precursor PAN fiber should be an organic solvent, which could be used to spin into an aqueous solution [6]. Reagent grade N,N-Dimethylacetamide (DMAc) from Fisher Scientific was chosen to be the solvent for this application. DMAc is a solvent for PAN and miscible in water. Water is not a solvent for PAN and therefore the water causes the PAN dope to coagulate and functions as a miscible non-solvent with the DMAc. Several polymers were used throughout this study, including polyacrylonitrile homopolymer (PAN) powder from Scientific Polymer Products, Inc. with a weight average molecular weight of 150,000 M_w and a copolymer of acrylonitrile and methylacrylate (PAN-co-MA) which had a viscosity average molecular weight of 250,000 M_v.

2.5.2 Dope Preparation

The dope was prepared using a custom built temperature controlled, zero head mixer, shown in Figure 2.10. Issues with fiber spinning stability are most often rooted in the presence of air bubbles incorporated into the spinning solution, as discussed previously, and must often be removed by placing the suspension, or resultant dope under vacuum for a period of time. Also related to fiber spinnability is the presence of undissolved polymer particles or gels [3], both of which lead either to fiber breakages, or point defects in the resultant fiber [6]. These issues are alleviated with the design of the dope mixer, which allowed for both heating and slow stirring of the dope at controlled rates while maintaining zero-head gas space above the contained dope. Thoroughly mixing the suspension while heating ensures full dissolution of the polymer into the solvent and a homogenous solution viscosity and minimal gel formation. Maintaining zero head space while mixing mitigates the formation of skin from dried polymer solution and eliminates the creation of air pockets in the solution. In order to mix, a stirrer is held on-axis with a pneumatic cylinder piston bearing, allowing for hydrostatic expansion and contraction of the dope as the plunger rises and falls during dissolution, heating, and cooling.

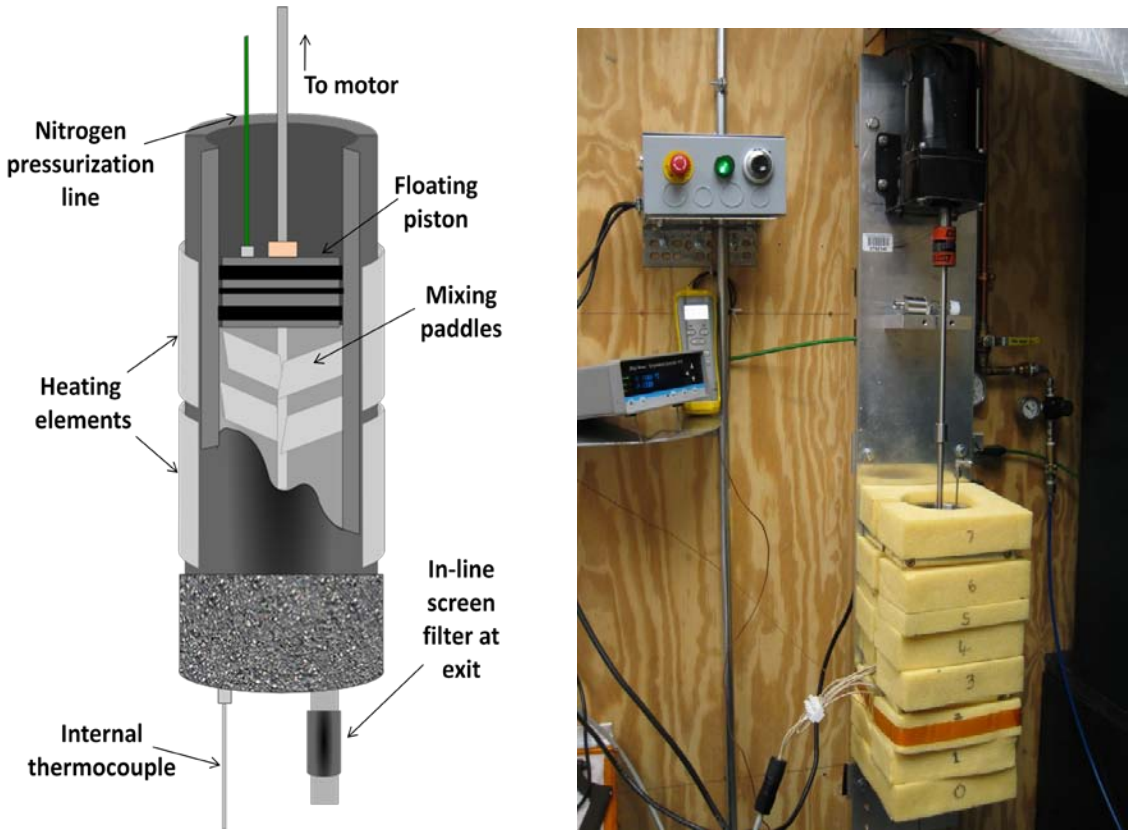

Figure 2.10. High volume custom built dope mixer

Typical wet-jet spinning solutions of 18 wt.% were found spinnable through experimentation and rheology standards, which will be discussed later. An 18 wt.% PAN/DMAc suspension, for example, was created by combining 800 g of dry N, N-Dimethylacetamide and 176.6 g PAN polymer. The suspension was then placed under a rotor-stator, Silverson lab mixer (L4RT) operated at 3000 rpm for 10 minutes with a 2 inch diameter, high shear screen in order to ensure a homogenous mixture. This suspension was then vacuumed to 29.9 in-Hg for 20 minutes and poured into the dope mixer, sealed, and the heating schedule followed as outlined in Table 2.1 (notice temperature set points were set per the control, not process, thermocouple), while stirring at ~8 rpm. This schedule allowed the internal temperature of the dope to reach a maximum of 117 °C, as seen in Figure 2.11.

Table 2.1. Control program for high volume dope mixer

Control Ramp and Soak Program
Ramp
155°C over 30 minutes
Hold
155°C for 2.5 hours
Ramp
60°C over 5 hours
Hold
60°C for 10 hours
Ramp
25°C over 4 hours
Hold
25°C off

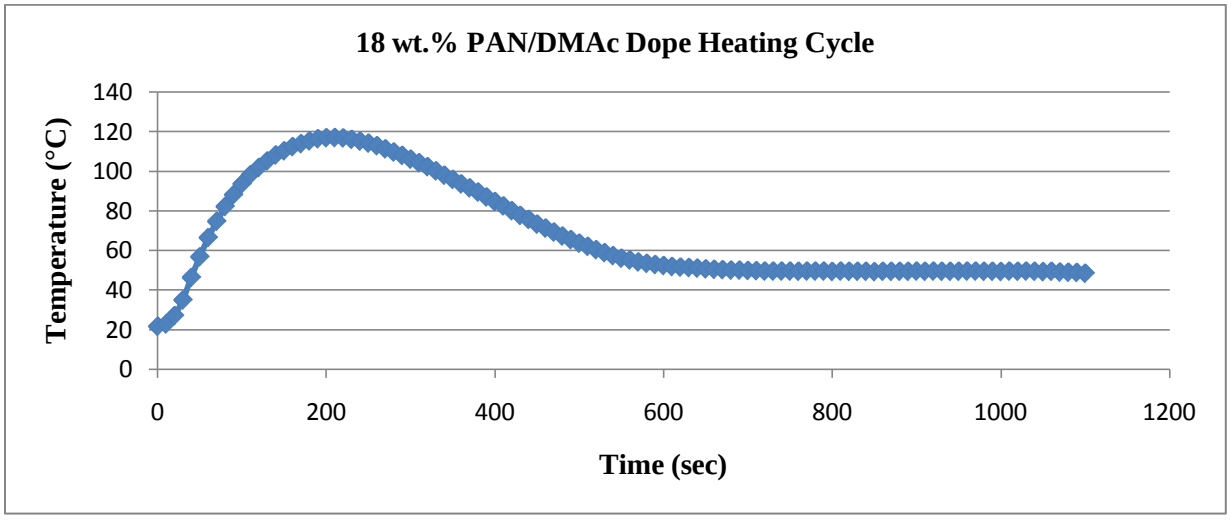

Figure 2.11. 18 wt.% PAN/DMAc dope heating cycle

It was found that the dope temperature must reach 100 °C and dwell above that temperature for at least 1 hour in order for the polymer to completely dissolve within the solvent. Improper heating, i.e. not reaching the preferred heating temperature, leads to a grainy appearance (due to undissolved or gelled polymer) and therefore a lack of "spinnability" and increased likelihood of clogging filters.

After the heating cycle, four KD Scientific 200 mL stainless steel syringes, fitted with Kalrez o-rings, were filled from the bottom of the mixer through a 140 micron in-line screen filter by locking the floating piston from rising and pressurizing the internal volume. The open syringes were then placed in a vacuum box for the removal of any dissolved gases. After the syringes were purged of all air, they were ready for integration into the dope metering pump inlet system.

2.6 Rheology

In order to specify a spinning standard, several dopes were rheologically investigated to establish a baseline viscosity for wet-spinning. Rheology is fundamental for the analysis of polymer fluids. Knowledge of how the fluid reacts under high shear stresses is invaluable when determining the necessary composition of the spinning dopes.

Rheology is pivotal in the description of the "spinnability" of the dope solution, or the ability to maintain a solution thread without breaking. Therefore, the ability to rheologically describe the spinning solution is essential for the development of improved spinning solutions.

2.6.1 Parallel-Plate Rheology

Producing a stable spinning process depends on a variety of factors, one of the most vital being the stable flow of spinning fluid through the spinnerette capillary. In order to produce stable flow of fluid through a capillary under tension, the fluid must maintain a certain viscosity. There are many ways to measure the viscosity of fluids, one of which is the motion of a fluid between two parallel plates. While the bottom plate is stationary, the top plate moves with a constant velocity, $\vec{v}$. Therefore, the fluid in contact with each surface has the same velocity as that surface, and the flow speeds of the intermediate layers of fluid increase uniformly from one surface to the other, in laminar flow. A portion of the fluid becomes more distorted as the motion continues. Therefore, the fluid is in a state of increasing shear strain. Forces, F, are applied to the top plate to keep it moving and a force, F, in the opposite direction is placed on the bottom plate, to hold it stationary, as in Figure 2.12.

If the plates have an area, A, then the shear stress is $^{F}/_{A} = \tau\ (Pa)$. The rate of change of strain, the strain rate, equals the speed *v* of the moving surface divided by *l* [29].

$$\text{Rate of change of shear strain = strain rate} = \frac{v}{l} = \dot{\gamma}\ \ (s^{-1})$$

The viscosity, η (Pa-sec), of the fluid is therefore defined as the ratio of the shear stress to the strain rate [29].

$$\eta = \frac{Shear\ stress}{Shear\ rate} = \frac{^{F}/_{A}}{^{v}/_{l}} = \frac{\tau}{\dot{\gamma}}$$

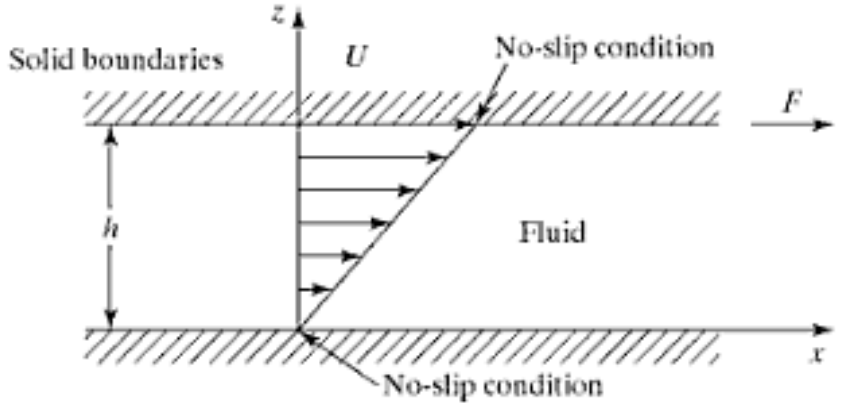

Figure 2.12. Laminar flow of a viscous fluid

(Copyright © 2010 Jodi Katz. Reprinted with the permission of Cambridge University Press) [30]

In order to evaluate these properties, a parallel-plate rheometer is often used, particularly at low shear rates [29]. A parallel-plate rheometer operates by rotating the top plate at a certain frequency while the bottom disc remains static, as seen in Figure 2.13. The rheometer then measures the torque in the flow field between the plates. In a steady shear experiment, viscosity is determined by measuring torque (M) in the torsional flow between two identical, parallel, coaxial discs. Varying the speed of rotation allows a range of shear rates to be investigated.

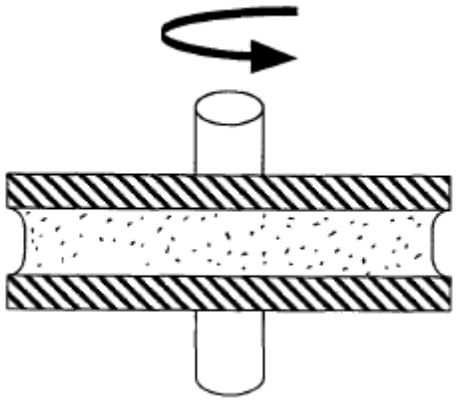

Figure 2.13. Schematic diagram of parallel-plate rheometer (Figure from Gupta) [29]

In order to determine dynamic properties, an oscillation mode may be used. In oscillation mode, a small-amplitude sinusoidal deformation is applied by one plate relative to the other at gap spacing, h. The angular strain amplitude (ϕ_0) is kept small to ensure the entire sample is within the linear viscoelastic region. By measuring the torque amplitude (M_0) and phase difference (δ) from the angular deformation, the storage (G') and loss modulus (G'') can be determined [29]. The equation for storage and loss modulus can be seen below.

$$G' = \frac{2M_0 h \cos \delta}{\pi R^4 \phi_0}$$

$$G'' = \frac{2M_0 h \sin \delta}{\pi R^4 \phi_0}$$

Steady-shear and oscillatory rheology were carried out on a TA Instruments AR-G2 rotational rheometer. Steady-shear data was collected for shear rates in the range of 0.1 to 10 s^{-1}. Oscillatory measurements, to obtain G', G'', and complex viscosity (η^*), were then completed for an angular frequency range from 0.1 to 100 rad/s at a controlled 0.01% strain.

These rheological experiments were carried out once a suitable dope composition was established via experimentation to determine the viscosity of the successful spinning solution. The optimum composition for wet-jet spinning was found by experimentation

to be an 18 wt.% PAN/DMAc solution. Shear rheology was performed on multiple 18 wt.% PAN/DMAc solutions provided by the purpose-built dope mixer (to ensure repeatability of results) and a 16 and 20 wt.% PAN/DMAc sample, with the results found below in Figure 2.14. The results showed that for the optimum concentration of 18 wt.% PAN/DMAc, the steady shear viscosity was approximately 80 Pa-sec at 1 1/sec shear rate. Concentrations of 16 and 20 wt.% PAN/DMAc are also shown and have lower and higher viscosities, respectively. Knowledge of the steady shear viscosity of an 18 wt.% PAN/DMAc solution as the optimum solution for wet-jet spinning allows for the determination of concentrations of various other polymers with a target goal of achieving approximately 80 Pa-sec at 1 1/sec shear rate for steady shear viscosity for wet-jet spinning.

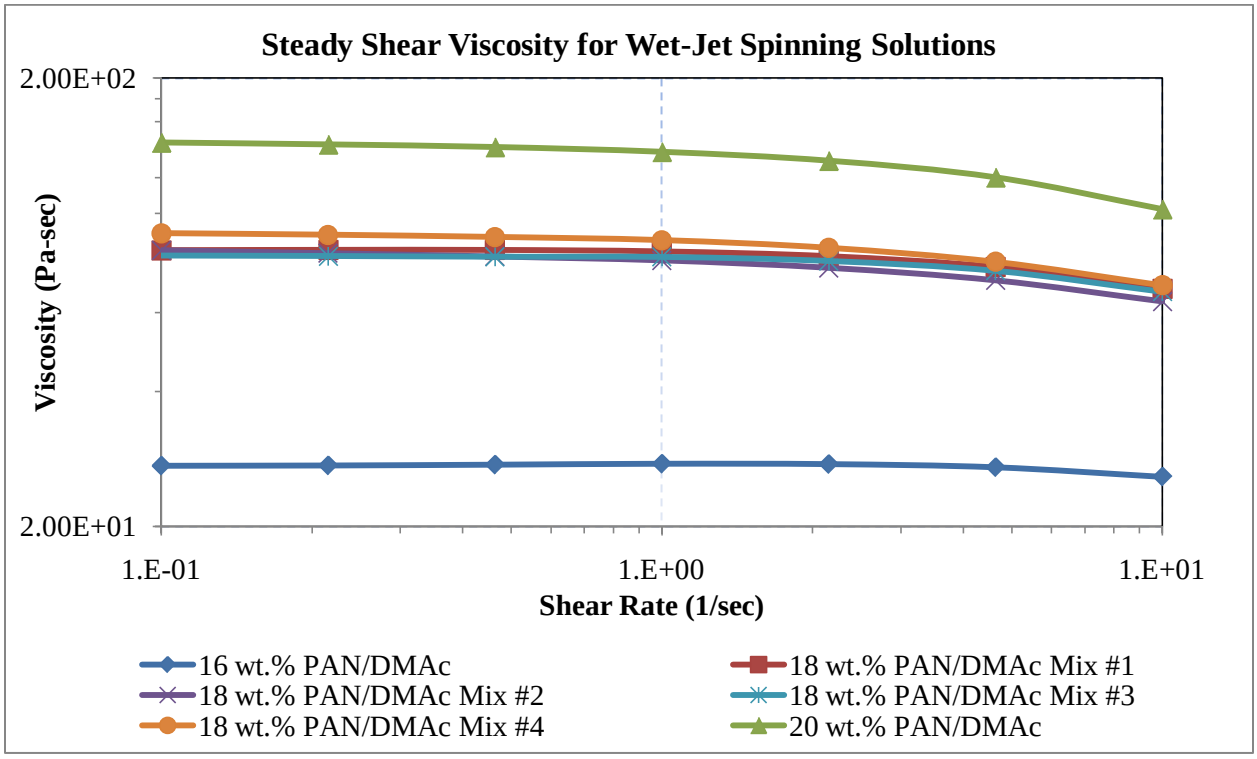

Figure 2.14. Steady shear viscosity of varying dope concentrations

2.6.2 Extensional Rheometry

Also important for the determination of the spinnability of spinning solutions is the extensional viscosity. Compared to shear viscosity, extensional viscosity can have values for resistance to flow orders of magnitude higher than shear. Materials that behave

identical or similarly in shear flow can behave completely differently in extensional flow. Extensional viscosity depends on a measurement of the force a fluid can withstand under uniaxial tension, as described in the equations below. For uniaxial extensional flow at a constant stretch rate, the fluid velocity v_1 in the direction of flow x_1 is

$$v_1 = \dot{\epsilon} x_1$$

Where $\dot{\epsilon}$ is the stretch rate. The velocity of the upper plate is equal to $^{dl}/_{dt}$ where *l* is the instantaneous filament length. Therefore,

$$^{dl}/_{dt} = \dot{\epsilon} l$$

Which, after integration, becomes

$$l = l_0 \exp(\dot{\epsilon} t)$$

This shows that the filament length increases with time, where l_0 is the initial separation of the discs. According to conservation of mass, the radius of the filament decreases from the initial value r_0 by

$$r = r_0 \exp\left(-\frac{\dot{\epsilon} t}{2}\right)$$

Therefore, the total stress, T_{zz}, in the axial direction at a distance z from the bottom plate is

$$T_{zz} = \frac{F_0}{A} - \rho g z - 2\gamma / r$$

Where F_0 is the force measured on the bottom plate, A is the cross sectional area of the filament, ρ is the density of the fluid being stretched, and γ is the surface tension of the fluid. The inertial and air drag forces on the stretching filament can be considered negligible [25]. Surface tension requires the total stress in the radial direction T_{rr} to be equal to

$$T_{rr} = -\gamma/r$$

And the extensional viscosity η_E of the fluid at the midpoint of the extending filament is defined by

$$\eta_E = \frac{T_{zz} - T_{rr}}{\dot{\epsilon}} = \left(\frac{F_0}{A} - \frac{\rho g l}{2} - \frac{\gamma}{r}\right)/\dot{\epsilon}$$

The results from the measurement of extensional viscosity of several samples are further described below and further quantify the spinnability of certain polymer solutions.

The extensional viscosity measurements were carried out using a Thermo Scientific HAAKE CaBER 1 extensional rheometer in collaboration with Professor Gerald G. Fuller at Stanford University. Use of the CaBER 1 requires placing a small sample of the spinning solution (<0.2 mL) between two circular plates. The top plate is separated from the bottom at a selected strain rate. After stretching, the fluid at the midpoint of the filament undergoes an extensional strain rate defined by the extensional properties of the fluid, as seen in Figure 2.15. This allows for the determination of extensional viscosity [31].

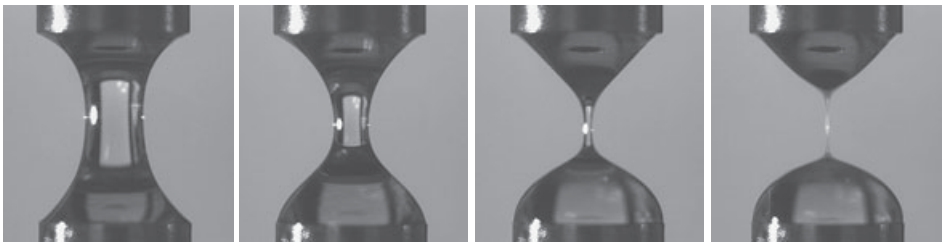

Figure 2.15. Extensional strain rate imposed on spinning solution (Figure from Thermo Scientific) [31]

Extensional flow rheology was carried out on the same solutions used in the steady state shear experiments mentioned in Figure 2.14. The 16, 18, and 20 wt.% PAN/DMAc solutions were analyzed, the results of which can be seen in Figure 2.16. Results show that the apparent extensional viscosity increases with increasing Hencky strain, which is defined as

$$\varepsilon_H = \ln\left(\frac{D_{mid}(t)}{D_1}\right)$$

Where $D_{mid}(t)$ is the diameter at the midpoint of the fluid with respect to time and D_1 is the initial fluid diameter. Hencky strain is also shown to decrease with increases in polymer concentration. This indicated that the solutions were able to tolerate greater increases in strain at lower polymer concentrations, therefore suggesting stable fiber spinning at low polymer concentrations.

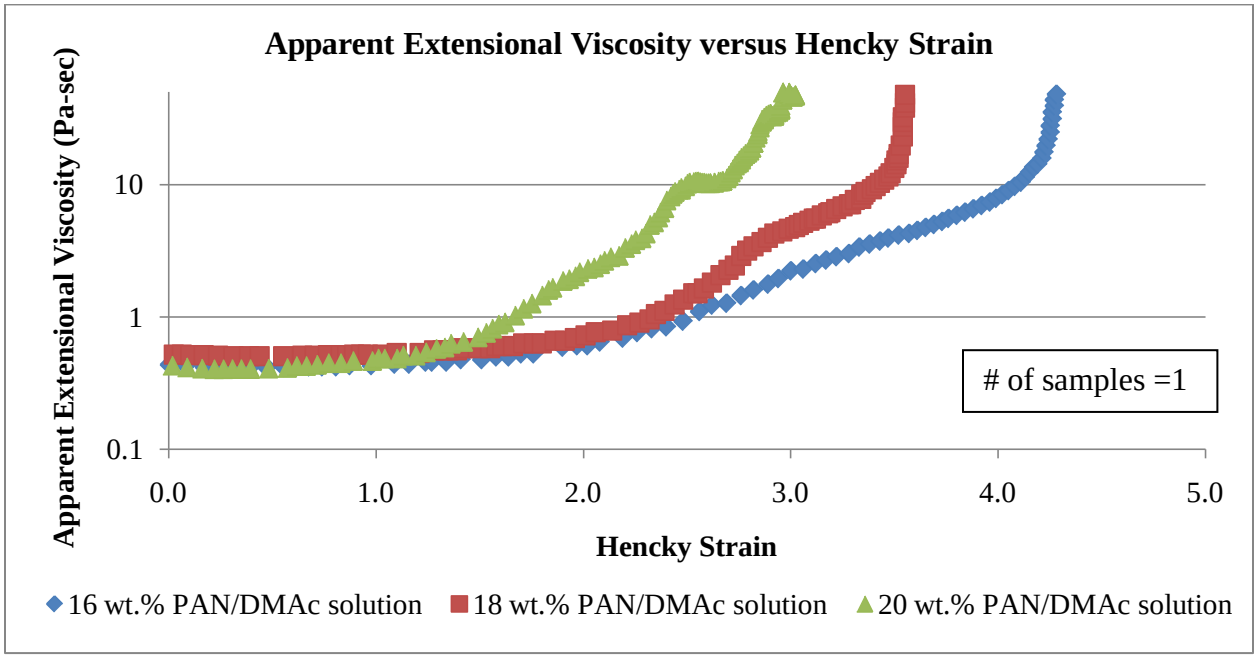

Figure 2.16. Apparent extensional viscosity versus Hencky strain

In conclusion, the use of parallel-plate rheometry as well as extensional rheometry allows for the determination of quantified limits in viscosities for proven polymer solutions. These quantified results allow for the formulation of new spinning dopes from other polymers for wet spinning.

3 Influence of Concentration and Temperature

3.1 Introduction

Coagulation plays a key role in the determination of the structure of precursor fibers, and it is this structure that influences the extent to which desirable properties can be developed in the final product. High quality PAN precursor has physical characteristics including a smaller diameter and consistent cross-sectional shape, which is preferably circular for optimum mechanical and physical properties of the final carbon fiber [5, 11, 32]. These physical characteristics are determined by the internal and surface properties of the precursor fiber, which are in turn affected by coagulation.

Coagulation occurs as the precursor fiber passes through baths containing a mixture of solvent and non-solvent, the percentage of solvent as well as the bath temperature used being based on the rate of coagulation desired. A concentration gradient is formed and osmosis occurs as the concentrations attempt to reach equilibrium. Therefore there is an influx of non-solvent from the bath into the fiber and a movement of solvent within the fiber to the bath. If the solvent leaves the fiber at a rate higher than the non-solvent entering the fiber, the cross-sectional shape of the fiber will depend on the mechanical behavior of the "skin" formed during coagulation. This skin is formed when coagulation occurs too quickly on the outer regions of the fiber. If the skin is rigid, as is the result at high rates of coagulation, the result will be a collapse in the cross-section leading to non-circular dog-bone shapes. However, if the rate of coagulation is controlled, the soft skin will shrink with the fiber, leading to a circular cross-section [32].

Craig discusses the affects of coagulation on the internal structure of the fiber, noting that several researchers have discovered a correlation between coagulation conditions and the porosity of the fiber as it relates to the coagulant, spinning solvent, and temperature of the coagulation baths. The porosity of the fiber was ultimately found to be attributed to internal stresses during coagulation, therefore leading to the conclusion that a slow and steady coagulation is best for producing fibers with maximum desirable properties [19]. Control and understanding of the coagulation rate and the associated effects has therefore been widely studied in the field of acrylic fibers. This chapter is a study of the effect of both coagulation bath concentration and temperature on fiber cross-sectional shape,

density, fibrillar structure and porosity. These experimental parameters were tested within the first coagulation bath, also known as the plunge bath. Fibers were wet-jet spun in 100 count tows using an 18 wt.% PAN/DMAc solution, as determined from previous experiments. The goal of the experiment was to 1) explore the effect of plunge bath concentration and temperature and 2) establish a baseline for the spinning of high quality precursor fiber, with a consistent circular cross-section, high density, and low porosity.

3.1.1 Effect of Diffusion on Coagulation Rate

For these tests, the 18 wt.% PAN/DMAc solutions described in Figure 2.14 were used. Fiber for freeze drying was collected at the first godet upon exiting the plunge bath. First to be determined, using optical microscopy, was the cross sectional shape of the fiber. The cross sectional shape of the fiber is highly affected by the rate of coagulation, which is determined by the rate of diffusion of solvent out of the fiber compared with the rate of diffusion of non-solvent into the fiber. For a cylinder of infinite length where diffusion occurs in the radial direction, Fick's second law for diffusion for a single component is:

$$\frac{\partial C}{\partial t} = \frac{1}{r}\frac{\partial}{\partial r}\left(rD\,\frac{\partial C}{\partial r}\right)$$

Here, c represents solvent or non-solvent concentration in mol/L, D is the diffusion coefficient in m^2/s, t is the time in seconds, and r is normal to the surface of the filament. Using an infinite concentration boundary condition at r = R, the above equation has to satisfy the following boundary conditions for a cylinder with radius R [11, 13].

$$C=C_0 \text{ for } 0 \le r \le R \text{ at } t = 0$$

$$C=C_\infty \text{ for } t \ge 0 \text{ at } r = R$$

$$\frac{\partial C}{\partial r} = 0 \text{ for } t \ge 0 \text{ at } r = 0$$

Where C_0 represents the initial concentration of the solvent or non-solvent inside the filament and C_∞ represents the equilibrium concentration. The diffusion of solvent and non-solvent in and out of the fiber is taken as two independent processes, with several authors solving the first equation for each process [11].

Solving the first equation based on the above boundary conditions to find the diffusion coefficient results in the following two equations. The equation for solvent diffusing out of the filament is given by:

$$\frac{M_t}{M_\infty} = 1 + 4\left(\frac{C_0}{C_\infty} - 1\right)\sum_{n=1}^{\infty}\frac{1}{\lambda_n^2}e^{-D\lambda_n^2 t/R^2}$$

For non-solvent diffusing into the filament, the equation is given by:

$$\frac{M_t}{M_\infty} = 1 - 4\sum_{n=1}^{\infty}\frac{1}{\lambda_n^2}e^{-D\lambda_n^2 t/R^2}$$

Where M_t is the amount of solvent or non-solvent inside the filament at time *t*, M_∞ is the amount inside at equilibrium and λ_n is the positive root satisfying the zero-order Bessel function [11]. The M values on the left side can be experimentally determined, while the solvent diffusion coefficient, D, can be determined computationally. This is done by calculating the value of Dt/R_2, and then ascertaining the corresponding D value relating to a definite value of *t* [33]. Experimental and theoretical results using the above equations show that as the solvent concentration in the coagulation bath decreases, the diffusion rate increases [13] and the rate of outward diffusion of solvent is more rapid than the inward diffusion of non-solvent [11].

3.2 Materials and methods

3.2.1 Plunge Bath Configuration

Tests were carried out varying the plunge bath concentration and temperature according to Table 3.1. The original intention was to vary the solvent concentration at 30, 50 and 70 wt.% DMAc/DI H_20. However, tests at the upper and lower temperature limits for a concentration of 70 wt.% showed an instant coalescing of the fiber tow upon leaving the spinnerette, due to the extremely low coagulation rate. Therefore, the concentration was backed down to 60 wt.% to aid in coagulation.

Table 3.1. Plunge bath composition and temperature experimental matrix

	30 wt.% DMAc/DI H_20	50 wt.% DMAc/DI H_20	60 wt.% DMAc/DI H_20
0 °C	X	X	X
25 °C	X	X	X
50 °C	X	X	

3.2.2 Freeze Drying Specimens

Preservation of the gel fiber structure prior to drying and collapse was vital for the study of fiber structure as it related to the coagulation variables [12, 19, 34]. The porous structure formed during wet spinning through the coagulation bath was not at equilibrium and had been found to slowly collapse over time, especially when liquid filling the pores evaporates. This led to a collapse of the fiber and loss of the porous structure present at the exit of the coagulation bath. Therefore, a process known as freeze drying, commonly used in biological studies to preserve structures in cells and tissues, was employed to preserve the fiber structure [12]. The freeze drying process used was similar to that utilized by Knudsen, Craig, and Law in which the as spun fiber was taken from the coagulation bath, washed in DI water for removal of residual DMAc and frozen in liquid nitrogen [7, 12, 15]. The samples were then transferred to a pre-cooled vessel, at approximately -20°C and placed under vacuum for approximately 24 hours in order for sublimation of the water to take place. The samples were then placed in a desiccator until needed. Freeze drying in order to preserve fiber structure has been found not only to impact porosity and fibril size measurements, but has a significant effect on density when compared to samples dried at room temperature [12].

3.3 Results

3.3.2 Effect of Coagulation Rate on Cross Sectional Shape

Coagulation rate has been found to have a significant impact on the cross sectional shape of the fiber. As stated previously, fibers are more circular at higher bath temperatures and higher solvent contents in the coagulation baths [32], therefore a critical balance must be found between increasing the bath temperature and concentration. This balance is

important because high temperatures increase inward diffusion which leads to fiber swell and the increase in concentration slows the formation of an outer skin; however, extremely slow rates of coagulation may lead to coalescing of fiber or decreased fiber stability during stretch. In order to test this balance experimentally, the matrix found in Table 3.1 was followed for the variation in temperature and bath composition of the plunge bath, the first coagulating bath the fiber enters upon exiting the spinnerette. It is equipped with a "plungeable" roller to maximize residence time within the bath. As stated previously, it was found that tests at a concentration of 70 wt.% DMAc/H_20 resulted in coalescing of the fiber upon exiting the die. A plunge bath concentration of 70 wt.% DMAc in water was therefore determined to be the upper limit on concentration.

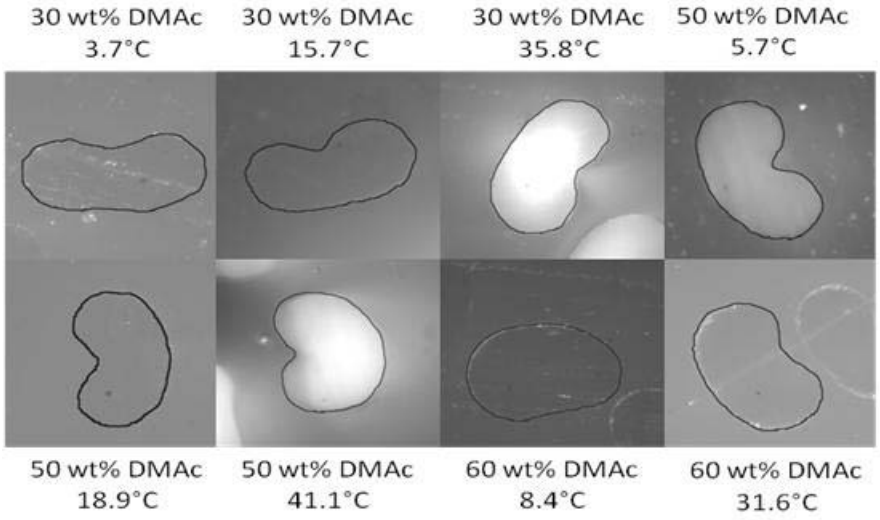

Figure 3.1. PAN fiber cross-sectional shape

The remaining experiments were carried out freeze drying fibers upon exiting the plunge bath and then embedding the fiber vertically in epoxy. The fibers were then analyzed using optical microscopy and the overall visual results presented in Figure 3.1. Deviation from fiber circularity has been found to affect mechanical properties [32], and several methods have been put forth to quantify circularity, including measurement of fiber width, ratio of cross-sectional area to the area of the circumscribed circle (or smallest area of perfect circle which can contain the fiber cross section), and the ratio of major and minor axes of the cross sections. Due to difficulty in applying the previous methods, it was determined that the method employed by Schloemer would be used [35]. Fiber

circularity, C, was therefore determined to be the roundness of the outer contour of the fiber regardless of the amount of lumen space included. Lumen space is defined as the missing area that would have been occupied by a full, round fiber, but is not occupied due to fiber collapse. Fullness, F, is a measure of the volume within the fiber as compared to the maximum volume it could contain if it were perfectly round and contains a correction for the void space [35]. The following two equations define the previous concepts.

$$C = \frac{4\pi A}{P^2}$$

$$F = \frac{4\pi (A - A_L)}{P^2}$$

Where

A = overall area of the cross section

A_L = area of the lumen cross section

P = perimeter of the cross section

A summary of the results using the above two equations to determine circularity and fullness can be seen in Table 3.2, with the highest circularity and fullness at 0.65 and 0.62, respectively, resulting from a plunge bath concentration of 60 wt.% at 8.4°C. Plots of the data are found in Figure 3.2 and Figure 3.3.

Table 3.2. PAN fiber circularity and fullness

Bath Concentration (wt.%)	Bath Temp (°C)	Circularity	Fullness
60	8.4	0.65	0.62
50	41.1	0.63	0.59
30	35.8	0.60	0.55
60	31.6	0.57	0.52
30	15.7	0.53	0.47
50	5.7	0.52	0.46
30	3.7	0.52	0.47
50	18.9	0.49	0.49

From Figure 3.2, it was found that at a 30 wt.% bath concentration, the circularity value increased steadily with temperature. Similarly, at a 50 wt.% concentration, although there was a slight dip in circularity values, overall, the circularity value also increased with temperature, resulting in overall higher values for circularity than the 30 wt.% concentration. This is in line with the theory that increasing solvent concentration and increasing temperature lead to more circular fibers. Interesting to note is the behavior of the fiber circularity at 60 wt.% bath concentration. Figure 3.2 shows that at a 60 wt.% concentration, the fiber circularity decreases with temperature. It was found in the earlier stages of the experimental design that fibers coagulated at 70 wt.% concentration and any temperature were not properly coagulated and therefore coalesced upon exiting the plunge bath. The same result was found for fibers collected at 60 wt.% concentration and high temperature. Therefore, it can be concluded that there is a practical limit to the high temperatures and high concentrations that can produce circular fibers. From these results, it can be determined that above 8.4 °C and 60 wt.% concentration, fiber coagulation is slowed to the point that the fiber structure begins to degrade. Similar results are found in Figure 3.3 for fiber fullness, showing a direct relation between fiber circularity and fullness.

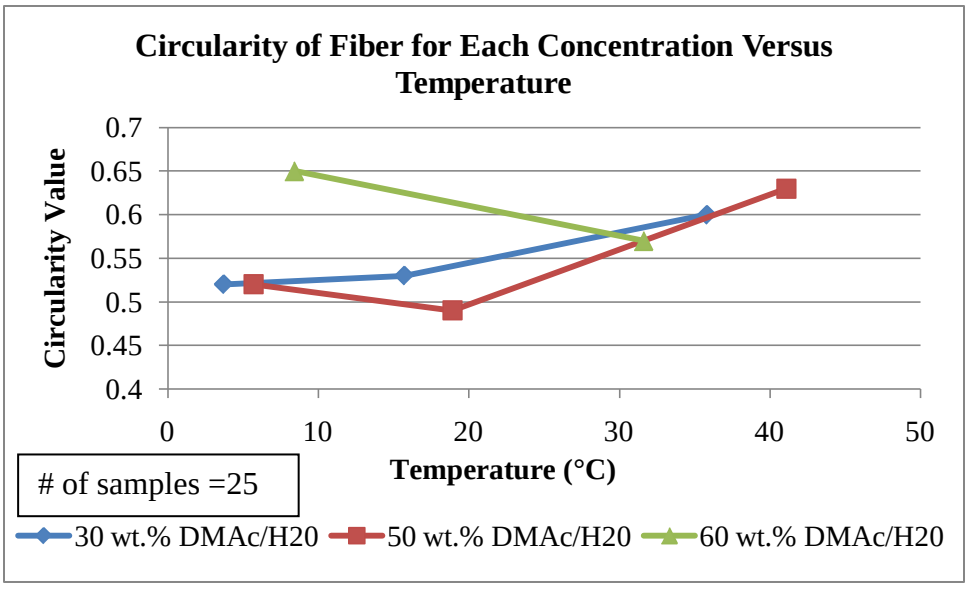

Figure 3.2. Circularity of fiber for each concentration versus temperature

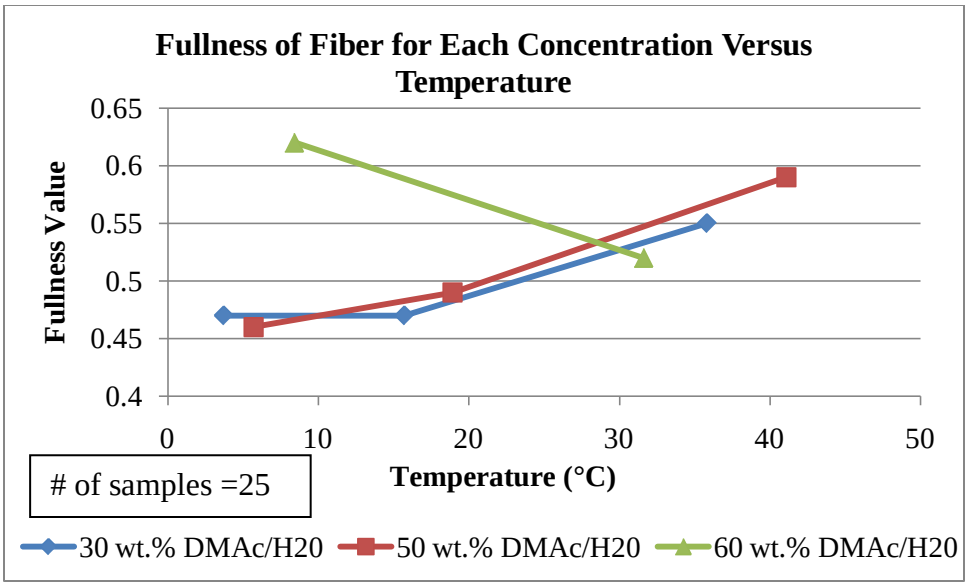

Figure 3.3. Fullness of fiber for each concentration versus temperature

3.3.1 Effect of Coagulation Rate on Void Content, Structure, and Density

Coagulation not only plays a critical role in the determination of fiber cross-section, but also in the development of voids within the fiber and therefore the resultant density. High void content and flaws have been shown to reduce the quality of the resultant carbon fiber [5, 18]. Therefore, fiber density is a good indicator of the ultimate properties of the fiber [16]. Thorne illustrated internal flaws present in acrylic fiber, noting the difference between void shape and particulate contamination. Cylindrical voids are stated to be gases dissolved in dope, while irregular voids are caused as a result of flow at the spinnerette, seen in Figure 3.4 [20]. The fibers collected above in Table 3.2 and analyzed for circularity and fullness are further analyzed for density and void content.

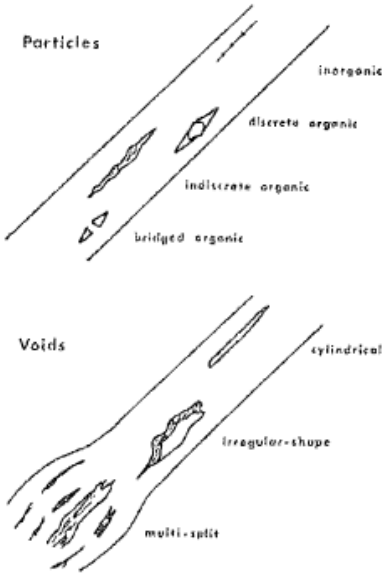

Figure 3.4. Types of internal flaws in acrylic polymer fibers (Figure from Thorne) [20]

The void content of the freeze-dried fiber was analyzed using optical microscopy of the fiber length by mounting fiber parallel on microscope slides and viewing the fiber perpendicular to the fiber axis. Fibers were viewed in reflected light, at a magnification of 500x in air, in Figure 3.5. Figure 3.5 shows the voids present in the fiber produced under conditions of 30 wt.% DMAc/H_20 bath composition at 35.8 °C.

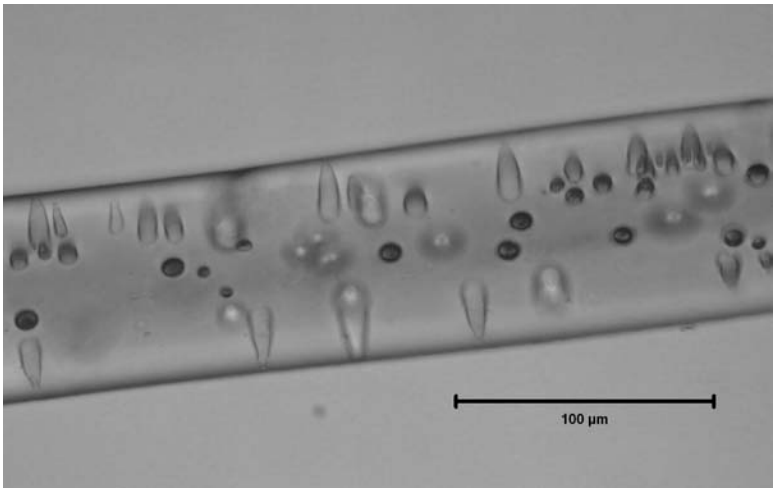

Figure 3.5. Void content of precursor PAN fiber

Figure 3.5 is consistent with the model proposed by Barnet in Figure 1.5. Elongated voids are arranged in a circular pattern about the cross section. The darker, more circular pockets seem consistent with entrained air within the dope solution. This experiment was carried out prior to pump customization to reduce the stream of bubbles being emitted in the spinning dope, as seen in Figure 2.3. Therefore, the presence of entrained air is likely due to the previous pump issue (which had not been addressed at this point) along with improper de-aeration of the spinning solutions prior to use and are therefore not formed by the coagulation process itself. Considering that the amount of solids and solvent within the spinning solution was kept constant for all experiments, as well as the spin draw, it can be inferred that the coagulation temperature and concentration had the greatest affect on these fibers. From the microscopy of other samples, higher bath solvent concentrations and lower temperatures lead to fewer voids within the fiber. Figure 3.6 shows an example of a fiber spun at 50 wt.% DMAc/H_20 and 5.7 °C which shows dominant voids to be caused by entrained air instead of voids caused due to coagulation stresses.

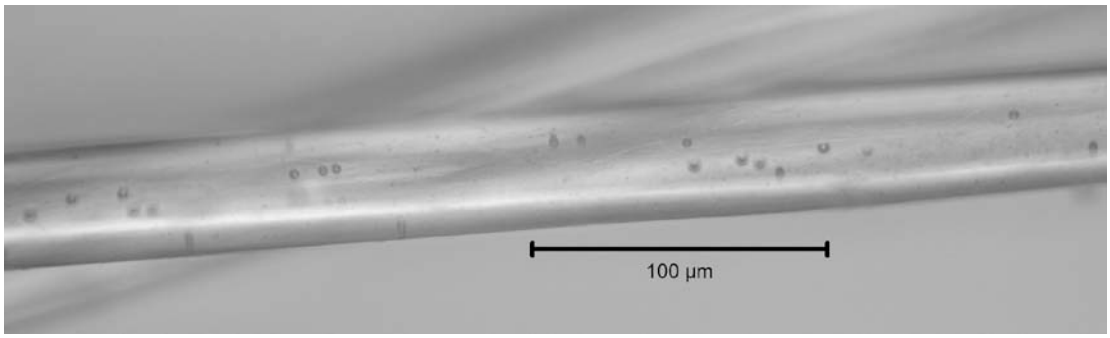

Figure 3.6. Entrained air within PAN precursor fiber

Major differences from the fiber seen above in Figure 3.6 and the fiber seen in Figure 3.5 include the absence of elongated voids. Present in the fiber in Figure 3.6, however, is entrained air, which can be identified as the random placement of very circular voids throughout the fiber cross section.

Further analysis of the fiber structure was completed using scanning electron microscopy (SEM). In order to properly cut the fiber to produce a clean cross section, care was taken to submerge the fiber completely in liquid nitrogen for a number of minutes, to ensure

freezing of the fiber structure throughout. A razor, also submerged in the liquid nitrogen, was then used to cut the fiber while remaining submerged. This provided a cleaner cut than previous methods. In order to prevent charging of the precursor fiber, it was gold sputtered prior to use in the SEM. Figure 3.7 shows an SEM image taken of the cross section of fiber spun in 30 wt.% DMAc/H_20 at 35.8 °C, the same conditions as that of the fiber in Figure 3.5. Concentric voids are again visible in the cross section, but more notably evident in this figure is the presence of a skin-core structure within the fiber. Again, this skin-core structure is explained by Heyi Ge, and also by Chen, as a multilayer structure [5, 11]. The mass transport is concentrated in the outer layers, which forms a dense layer in a short time, while the speed of inner layers of diffusion is slow, resulting in a loose inner layer [11]. Balancing the ratios between the layers is essential for producing a precursor fiber capable of effectively transmitting tensile forces throughout the fiber. Therefore, low solvent concentration of coagulation bath and high coagulation temperatures are not valuable for producing such a high performance PAN precursor.

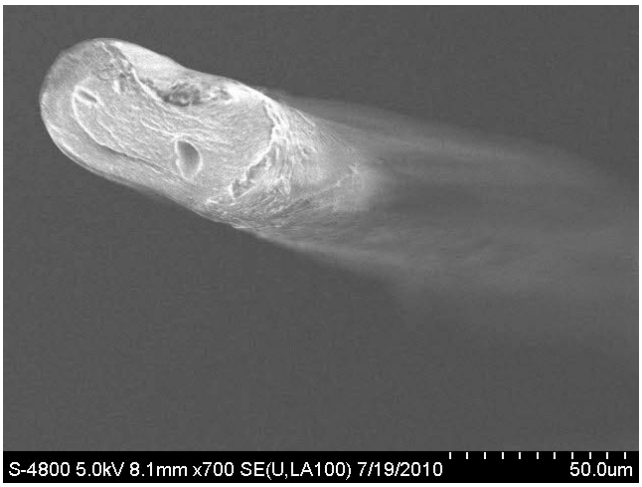

Figure 3.7. SEM image of skin-core structure of PAN precursor fiber produced at 30wt% DMAc/H_20 and 35.8°C

Aside from void development, the density of the fiber plays an important role in the resultant carbon fiber properties. Fiber density can also be an indicator of the number of voids present within the fiber, as well as the loose fibrillar structure. It is an important determining factor for the fiber strength and modulus. Density measurements were performed on numerous fibers using ASTM D3800 Standard Test Method for Density of

High-Modulus Fibers. The procedure uses the buoyancy (Archimedes) method to determine density, first weighing the sample in air and then weighing in a wetting liquid with a lower density. Some important aspects to consider: liquid temperature tolerance of ±1°C, removal of entrapped air in sample bundle, sample distance lowered into liquid remain same, and the sample sizes should be within a few grams from one sample to another. The general apparatus set up can be seen in Figure 3.8. The actual experimental setup included a balance accurate to four significant digits placed directly over a 500 mL beaker. The beaker was placed on a lab jack for simple height adjustment. Acetone was found to be the most appropriate wetting fluid, as the use of water caused the fiber bundle to float and did not sufficiently wet the sample.

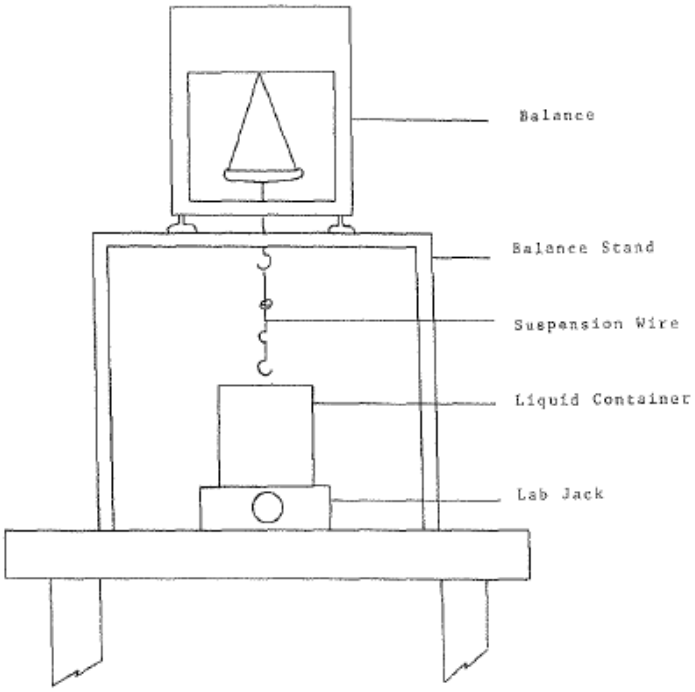

Figure 3.8. Density apparatus (Figure from ASTM D3800)

In order to calculate the density of the fiber, the following equation was used.

$$\rho_f = (M_3 - M_1)\rho_l/((M_3 - M_1) - (M_4 - M_2))$$

M_1= weight of suspension wire (grams)

M_2= weight of suspension wire immersed in liquid to immersion point (grams)

M_3=weight of fiber sample and wire (grams)

M_4=weight of fiber sample and wire immersed in liquid to immersion point (grams)

Where

$$\rho_l = \rho_s((M_3 - M_1) - (M_4 - M_2))/(M_3 - M_1)$$

and

$$\rho_s = \frac{(M_3 - M_1)\rho_w}{((M_3 - M_1)} - (M_4 - M_2))$$

Here, ρ_w is the density of water used for calculating the density of the standard and ρ_s is the density of the standard. In this case, the standard was a Troemner ASTM class 1 stainless steel 1 gram weight with a noted density of 7.85 g/cm^3. The average density for the standard in water was found to be 7.0678 g/ cm^3 with a standard deviation of 0.0054 g/ cm^3. The use of water as the wetting fluid was not possible due to the buoyancy of the fiber within the water. Therefore, according to the ASTM Standard, the next acceptable wetting fluid was acetone, which was found to fully wet the fiber during density measurement. The use of the known density of acetone was acceptable and did not need to be calculated.

$$\rho_{l_{acetone}} = 0.785\ g/cm^3$$

This density and the masses measured were used to calculate the densities of the fiber. The average temperature for the acetone used during measuring was 23.6±0.8°C. Due to the small amounts of fiber collected during the previous experiment, the density measurements were only carried out once. The results of the density measurements can be seen in Table 3.3.

Table 3.3. Density of precursor fiber spun at varying temperatures and coagulation conditions

Density (g/cm^3)	Temp (°C)	Wt.% DMAc/H20
1.0292	35.8	30
1.0853	5.7	50
1.1059	18.9	50
1.1155	41.1	50
1.1345	8.4	60
1.1431	31.6	60
1.1441	3.7	30
1.1465	15.7	30

As seen from Table 3.3, the lowest density fiber resulted from fiber spun in 30 wt.% DMAc/H_20 at 35.8 °C, which is consistent with the numerous void structures seen in Figure 3.5. A high number of voids within the fiber should lower the density and indicate a weak precursor fiber. The highest density was found in the fiber spun at 15.7 °C in 30 w.% DMAc/H_20. The results in Figure 3.9 show the densities plotted versus temperature. Other than the outlier at 30 wt.% DMAc/H_20 and 35.8 °C, density is seen to increase with temperature.

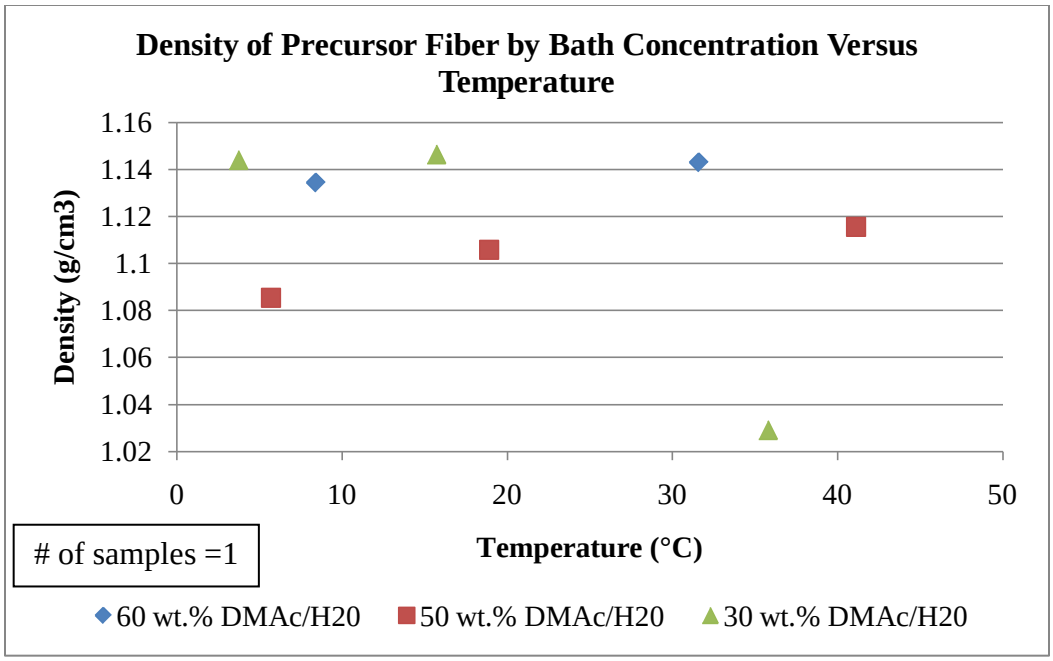

Figure 3.9. Density of precursor fiber by bath concentration versus temperature

One explanation for this phenomenon may have to do with the type of voids present in the fiber. Although a fiber may have an increased number of voids due to high temperature coagulation, some of those peripheral voids may be open to the wetting fluid, filling with wetting fluid during density measurement. Therefore, any voids that fill with wetting fluid, or in this case acetone, would appear denser than internal voids, such as the entrained air seen in Figure 3.6. Further, the test method states that any entrapped air will change the material density and not give a true density reading. Therefore, the fiber coagulated at higher temperatures may in fact contain a higher number of voids, as demonstrated by Figure 3.5, but not show this result with the given density measurement method. In order to properly find the density of these fibers without penetration of the fluid into the peripheral voids, a non-wetting fluid with a higher surface tension should be used, such as mercury, with a surface tension of 425 mN/m. According to the Kelvin equation, mercury will not penetrate a void smaller than 6 μm in radius [19]. Compared to the surface tension of acetone, which is only 25 mN/m, this may significantly increase the accuracy of the density results.

Regarding bath concentration, the results in Figure 3.9 show the fiber density to be independent of bath concentration. This has been found in several previous studies, including a study by Knudsen which measured the densities of several fibers spun into baths of varying concentrations and found little difference [12]. It can be concluded that bath temperature has a greater effect on density than bath concentration.

There are many factors which affect the fiber density, including void content, as discussed previously, and also the presence of residual solvent, or DMAc, within the fiber. As the fiber coagulates slowly through the progression of baths, the ultimate goal is to remove all of the DMAc from the fiber, leaving behind only polymer. However, if coagulation proceeds too quickly, causing a thick outer skin to form, residual DMAc will become trapped within the fiber. Knudsen found that this indicates the existence of non-communicating voids in the fiber [15]. Due to this affect on the fiber, residual DMAc measurements were undertaken using gas chromatography. Gas chromatography (GC) is the most appropriate specific solvent analysis. It has the ability to separate component solvents and identify them. For known solvent determinations, the flame ionization detector (FID) is adequate due to its low detection limits, dynamic range, and reliability for trace organic compounds. Capillary GC columns have a high resolution and low detection limits and are most often used with trace organic volatile analysis [36]. For the current analysis, an HP-Innowax column measuring 30 m x 0.25 mm x 0.25 μm was used. Flow was set at 3.27 mL/min with a ramp from 110 °C to 225 °C at 7 °C/min.

For residual solvent analysis, fiber was spun using an 18 wt.% PAN/DMAc solution and collected after each coagulation bath. Fiber was allowed to spool for 1 minute onto the godet roller and was then carefully cut from the roller and placed on a Kimwipe. The Kimwipe was then systematically pressed over the fiber for 1 minute to remove excess solution, as seen in Figure 3.10. Care was taken to ensure even distribution of force over fiber during solution removal. Following removal of excess solution, the fibers were placed into previously tared 250 mL bottles and the masses of the bottles and fiber weighed as one. Deionized water was then added to each bottle, as seen in Figure 3.11.

The bottles sat for 24 hours to allow the solvent to diffuse from the fiber. Samples were then taken from each bottle and run in the GC as stated above. Calibration standards were also developed by placing varying amounts of trace DMAc in deionized water and testing on the GC for accuracy of the GC results.

Figure 3.10. Excess solution removed from fiber using a Kimwipe

Figure 3.11. Deionized water added to fiber in 250 mL bottle

The residence time of the fiber in each coagulation bath prior to take-up on the following godet was necessary to calculate in order to determine the effect on the residual DMAc within the fiber at each point. The results can be seen in Table 3.4. The residence time per bath was calculated using the following equation.

$$\frac{Dist.\,Btw\ Ceramic\ Rollers\ (m)}{Godet\ Speed\ \left(\frac{m}{\min}\right)} \times \frac{60\ sec}{1\ min} = Residence\ Time\ per\ Bath\ (\text{sec})$$

The total residence time therefore became the sum of all previous residence times.

Table 3.4. Residence time of fiber between godets

Godet Speed (m/min)	Dist. Btw Ceramic Rollers (m)	Residence Time per Bath (sec)	Total Residence Time (sec)
0.98	1.36	83.27	83.27
1.99	2.24	67.54	150.80
2.18	2.2	60.55	211.35
2.28	2.15	56.58	267.93
2.39	2.13	53.47	321.41
2.6	2.21	51.00	372.41
2.62	2.14	49.01	421.41
2.67	2.08	46.74	468.15
7.37	2.16	17.58	485.74

Using the results of the GC for the weight percent DMAc in each of the solutions, it was possible to calculate the weight percent DMAc in the fiber at each stage along the spinline. Knowing the amount of fiber in each bottle, along with the amount of H_2O and DMAc, the following equation could be used to discern the amount of DMAc in the fiber.

$$\frac{GC\ Meas.Wt.\%\ DMAc\ (g)}{100} \times [H_20 + DMAc\ (g)] = \text{DMAc (g)}$$

Once the amount of DMAc within the fiber was known, that amount could be divided by the amount of fiber and multiplied by 100 to get the weight percent DMAc in the fiber. The results of these calculations can be seen in Table 3.5, with a graph in Figure 3.12 showing the relationship between total residence time and residual DMAc weight percent.

Table 3.5. Determination of weight percent DMAc in fiber

	* assume (g) DMAc is negligible compared to H_2O (g)			
Fiber (g)	H_2O + DMAc* (g)	GC Meas. Wt.% DMAc	DMAc (g)	Wt.% DMAc in Fiber
2.74	160.87	0.72	1.15	42.07%
4.44	157.54	1.10	1.73	38.88%
4.59	163.96	1.01	1.66	36.09%
4.05	162.42	0.72	1.17	28.96%
3.85	159.96	0.65	1.04	27.04%
3.81	162.49	0.51	0.84	21.90%
3.60	167.76	0.35	0.59	16.28%
4.07	156.83	0.12	0.18	4.51%
1.90	169.40	0.01	0.02	1.21%

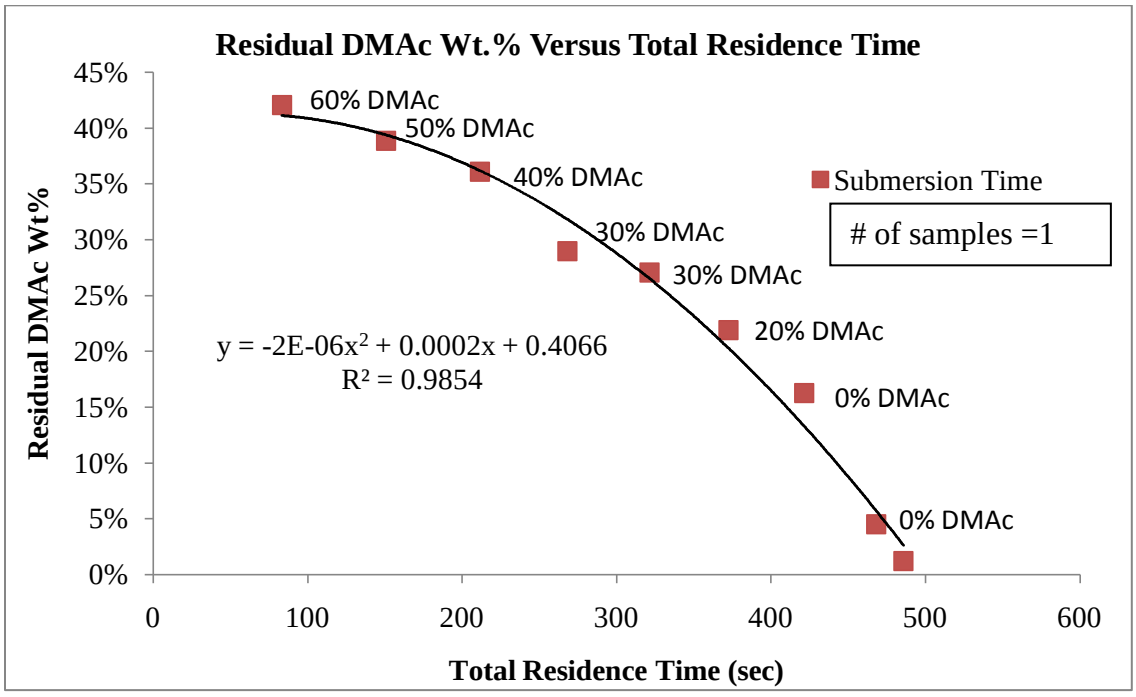

Figure 3.12. Residual DMAc wt.% versus total residence time

Figure 3.12 shows the gradual decrease in residual DMAc as the fiber progresses through each coagulation bath, with the actual bath concentration shown to the side of the data point. The coagulation is slow, gradual, and results in a final residual content of only

1.21%, indicating the number of baths and selection of concentrations to be necessary to gradual coagulation and ultimately a better fiber. It is important to note that the above residual solvent results are valid only for the godet speeds found in Table 3.4. Differences from these speeds result in changes in residence time of the fiber within the respective baths and leads to changes in the rate of coagulation. A decrease in the overall residence time leads to a flattening of the residual DMAc curve and will indicate higher amounts of solvent residing within the fiber at the end of the line, as concentration, temperature, and time all affect the rate of diffusion within the fiber.

3.4 Conclusions

After reviewing the previous experiments, the role coagulation and temperature play in the development of a high quality PAN precursor is apparent. As stated previously, high quality PAN precursor is characterized by a circular cross section, small diameter, and consistent cross sectional shape. In order to achieve these goals, diffusion must be understood and controlled in order to prevent a solid skin-core structure from forming. Also highly affected by the diffusion rate is the porosity of the fiber, which if left unchecked, can lead to a weak, highly porous fiber.

While some have postulated that fibers are more circular at higher bath temperatures and higher solvent contents in the coagulation baths, it was found that there is a practical limit to the high temperatures and high concentrations that can produce circular fibers. From the results, it was determined that above 8.4 °C and 60 wt.% concentration, fiber coagulation is slowed to the point that the fiber structure begins to degrade. Low coagulation temperatures have also been postulated to lead to a reduction in void content and increased density and fiber strength. Through experimentation, it was determined that low coagulation temperatures indeed produce a fiber with fewer voids, however, density was found to increase with increasing temperature due to the presence of communicating voids that fill with wetting fluid. Also present in the majority of the experimental fibers is entrained air, which must be minimized through proper vacuum de-aeration of the PAN/DMAc suspension prior to heating into solution. The density results determined through experimentation presented the top two densest fibers produced at 3.7 and 15.7 °C, both at 30 wt.% DMAc/H_20. In order to analyze the coagulation of the fiber as it

proceeds down the spinline, the residual DMAc content of the fiber was analyzed and showed a final residual content of 1.21 wt.% DMAc. This demonstrates smooth, gentle, and homogenous coagulation as the fiber moves down the line.

In conclusion, to produce a high quality precursor with circular cross section, high density, and low void content, the preferred coagulation conditions were found to be at low temperature and high concentration of solvent in the coagulation bath.

4 Development of Small Diameter Fiber

4.1 Introduction

According to the Griffith theory of fracture, a fiber consisting of a single molecule would possess the theoretical molecular tensile strength. This is due to the inability of a single molecule to possess defects or impurities, which lead to cracks, and ultimately fiber failure [21]. From this statement, one can come to the conclusion that the smallest possible fiber would allow for the smallest number of defects and impurities. Therefore, the development of high strength PAN fiber requires the development of a small diameter fiber.

4.2 Dry-Jet Wet Spinning

Research was carried out to develop a dry-jet wet spinning process using the current technology. The spinnerette design, seen in Figure 4.1, utilized a 100 filament, 150 micron capillary diameter design with an L/D=10 to encourage establishment of laminar flow through the capillary.

Figure 4.1. Dry-jet wet spinning die with 100 filament, 150 micron capillaries

Dry-jet wet spinning is preferred to wet jet spinning due to the increased spin draw available. In essence, the use of the air gap in dry-jet spinning means the fluid moving through this air gap has zero modulus, and can therefore withstand much higher rates of deformation. This allows for increased processing speeds. Experimentally, it has been determined that fibers spun using the dry-jet wet spinning technique are higher in luster due to the presence of fewer surface defects which are minimized in the air gap. During wet spinning, it is proposed that small defects in the capillaries of the spinnerette lead to small defects in the fiber as it exits the capillary. This, along with high stress at the die face, leads to increased defects in the fiber [3]. Since the filament instantly exits the spinnerette and enters the coagulant, this structure, defects included, is preserved. The use of the air-gap in dry-jet wet spinning allows for the correction of these defects as the fiber passes through the air-gap, effectively "sealing" any defects that may have existed as the fiber flows from the capillary, through the air-gap, and into the coagulant. Previous work has shown that fibers with fewer defects produces fiber with higher tensile strength [2, 5-7, 21].

Dry-jet wet spinning is also critical in the production of small diameter fiber. Due to the increased spin draw available during dry-jet spinning, the fiber is able to begin coagulating at a lower diameter than at the exit of the capillary. As can be seen in the following figure, as the dope exits the spinnerette capillary, there is a degree of die swell, which can be seen over the length L_0.

This die swell results in a larger initial diameter as the fiber instantly coagulates and preserves its form during wet spinning. Dry-jet wet spinning, however, allows the initial fiber form to be preserved at a lower diameter, as seen in Figure 4.2. Over the distance L_A, the fiber is pulled to a finer point, before finally entering the coagulant [37].

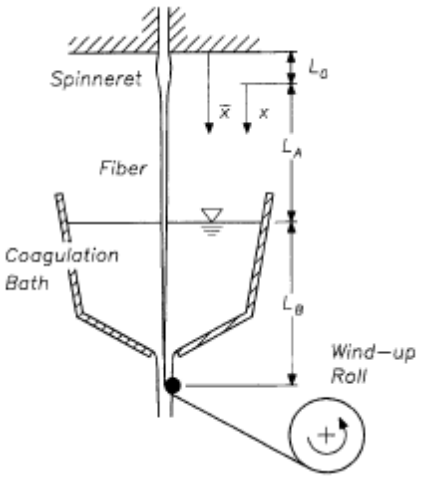

Figure 4.2. Dry-jet wet spinning process (Figure from Simon) [37]

4.3 Effect of Processing Parameters on Fiber Diameter

In order to develop a method for consistently spinning small diameter fiber, it became important to understand the mechanisms behind each part of the spinning process and how it impacted fiber diameter. First to be analyzed was the effect of the stretch, spin draw, and total draw down ratio on diameter. The stretch is the measure of fiber stretching over the entire spinning line, excluding the spin draw, and is described by the following equation.

$$Stretch = \prod_{y_0}^{y_{10}} DDR$$

The spin draw measures only the stretch found between the die face and the first godet, y_0. The spin draw is described by the following equation.

$$Spin\ draw = \frac{y_0}{Fluid\ velocity\ \left(\frac{m}{\min}\right)}$$

The total draw down ratio is the product of the spin draw and stretch.

A comparison of the total draw down ratio for several different wet-jet spinning runs can be seen below in Table 4.1. There is an evident relationship between increasing the draw down ratio and decreasing diameter, as would be expected.

Table 4.1. Total draw down ratio versus diameter for wet-jet spinning

Total DDR	Diameter (micron)
5.94	22.36
11.88	21.15
14.56	14.9
15.21	14.9

In an effort to increase the total DDR, a hot glycerol stretch bath was introduced at the end of the line prior to take-up. The hot glycerol is thought to give greater mobility to molecules allowing for relaxation and, under tension, alignment of molecules. With the addition of the hot glycerol bath, the total DDR increased to 24.75, with a resulting 10.44 micron fiber diameter. However, the glycerol proved messy, and difficult to remove from the fiber. Therefore, the implementation of a steam stretch as seen in Figure 4.3 replaced the glycerol. The steam stretch was designed by placing heaters in a shallow amount of water near the bottom of the bath. This water then boils, evaporating upward through a metal screen with yet another heater attached, effectively super-heating the steam to temperatures around 220 °C with the lid in place. The previous glycerol bath reached a maximum of only 145 °C. For wet-jet spinning, the results can be found in Table 4.2, with steam providing a much higher DDR with smaller diameter than the previous system, with and without glycerol stretching.

Table 4.2. Total draw down ratio versus diameter for wet-jet spinning with steam stretch

Total DDR	Diameter (micron)
6.73	18
19.71	9.32
24.04	8.08

Figure 4.3. Hot steam stretch bath (shown without top in place)

In conclusion, it was found that to produce the smallest fiber with the cleanest method, the steam stretch worked well.

After determining the most effective method, it was also necessary to analyze the effect of spin draw, stretch, and total DDR individually with respect to their effect on fiber diameter. The results can be seen in Table 4.3.

Table 4.3. Spin draw, stretch, and total DDR and respective fiber diameters

Spin draw	Stretch	Total DDR	Diameter (micron)
1.03	5.77	5.94	22.36
2.06	5.77	11.88	21.15
1.36	4.95	6.73	18
3.78	3.85	14.56	14.9
3.78	4.02	15.21	14.9
3.44	7.21	24.75	10.44
2.57	3.83	9.85	9.32
6.27	3.83	24.04	8.08

Table 4.3 shows which of the three variables has the most consistent effect on diameter. The total DDR is shown varying widely in its determination of diameter, while stretch is much more consistent. Stretch, however, shows a wavering ratio with decreasing diameter, moving lower and then moving higher. Spin draw is the most consistent

predictor of diameter, with ratio values increasing (for the most part) with decreasing diameter. This is due to the spin draw being the large single contributed to the overall total DDR, as total DDR is the product of spin draw and stretch ratios. Also, when referencing Figure 3.12, it is obvious that the slope of the plot of residual DMAc weight percent versus time increases over time, with the slope being the lowest between the first (plunge) and second baths. This shows that the rate of diffusion is low within the first bath due to the fiber structure being set within the first bath. The remaining baths serve to wash and remove excess solvent from the fiber. Therefore, it can be concluded that the production of small diameter fibers requires a high spin draw. This is logical due to the fact that much of the fiber structure is set within the first coagulating bath, where the spin draw takes place.

In the pursuit of a small diameter fiber, an experiment was carried out to compare the results of dry-jet and wet-jet wet spinning. The interest was in determining if maintaining the same spin draw and draw ratio on fiber would produce similar results between dry-jet and wet-jet spinning. To begin, appropriate fluid velocities were calculated, in order to maintain similar fluid exit velocities through different sized capillaries.

The wet-jet die used consisted of 100 capillaries measuring 60 micron in diameter ($\emptyset_{wet}$). The dry-jet die, as described, consisted of 100 capillaries measuring 150 micron in diameter ($\emptyset_{dry}$). Using the following equation, it was possible to determine the appropriate pump rates to maintain constant fluid exit velocity (at 0.16 cc/rev) to be 5 rpm for wet-jet spinning and 31.25 rpm for dry-jet spinning.

$$\frac{\emptyset_{wet}^2}{\emptyset_{dry}^2} = \frac{rpm_{wet}}{rpm_{dry}}$$

The wet-jet spinning run was completed first, spinning 20 wt.% PAN-co-MA/DMAc dope. The godet speeds can be seen in Table 4.4 below, with Table 4.4 also showing the wet-jet pump speed and Table 4.5 showing the dry-jet pump speed. Table 4.6 shows the spin draw, the stretch, and the total DDR for both the wet-jet and dry-jet spinning conditions, while Table 4.7 shows the bath compositions and temperatures.

Table 4.4. Godets speeds and draw down ratio for each godet during wet-jet spinning

Godet	Pump (rpm)	y_0	y_1	y_2	y_3	y_4	y_5	y_6	y_7	y_8	y_9	Heated Godet	y_{10}
Speed (dial setting)	5	1.50	1.00	1.05	1.05	1.05	1.10	1.00	1.40	0.70	1.27	0.93	2.77
Speed (meters/min)	1	1.36	2.89	3.04	3.03	3.04	3.20	2.89	3.21	7.29	6.70	7.12	6.73
DDR		1.36	2.13	1.05	1.00	1.00	1.05	0.90	1.11	2.27	0.92	1.06	0.95

Table 4.5. Godets speeds and draw down ratio for each godet during dry-jet spinning

Godet	Pump (rpm)	y_0	y_1	y_2	y_3	y_4	y_5	y_6	y_7	y_8	y_9	Heated Godet	y_{10}
Speed (dial setting)	31.25	1.50	1.00	1.05	1.05	1.05	1.10	1.00	1.40	0.70	1.27	0.93	2.77
Speed (meters/min)	1	1.36	2.89	3.04	3.03	3.04	3.20	2.89	3.21	7.29	6.70	7.12	6.73
DDR		1.36	2.13	1.05	1.00	1.00	1.05	0.90	1.11	2.27	0.92	1.06	0.95

Table 4.6. Spin draw, spin draw, and total draw down ratios for wet-jet and dry-jet spinning

Spin draw	Stretch	TOTAL DDR
1.36	6.73	9.16

Table 4.7. Bath composition and temperature

Bath	0	1	2	3	4	5	6	7	8
Composition (wt.% DMAc in H_20)	60	50	40	30	30	20	10	0	0
Temperature (°C)	8.3	6	10.6	15	19.4	24.1	28.3	31.1	82.2

Spinning was completed utilizing two different stretching temperatures. One spool of fiber was taken up at 107 °C, seen in Figure 4.4, and another at 212 °C, seen in Figure 4.5, to compare the effects of increasing stretch temperature.

Figure 4.4. Wet-jet spun fiber stretched at 107 °C

Figure 4.5. Wet-jet spun fiber stretched at 212 °C

After gathering spools of wet-spun fiber, the pump was stopped and the die replaced with the dry-jet spinning die, the pump turned up to 31.25 rpm and spinning resumed. All godets speeds were unchanged from the values seen in Table 4.4. Fiber was noticeably slack during dry-jet spinning, which will be discussed later. Again, two spools were gathered, one at 110 °C (Figure 4.6) and one at 220 °C (Figure 4.7).

Figure 4.6. Dry-jet spun fiber stretched at 110 °C

Figure 4.7. Dry-jet spun fiber stretched at 220 °C

The fibers were all analyzed using optical microscopy for diameter. Fibers were first embedded vertically into epoxy and polished, for optimum viewing. Fibers were viewed in 40 x oil using reflected light. After determining the diameter, single filament tensile testing was performed using a MTS QTest10 Elite with a 150 gram load cell. The test had a data acquisition rate of 10 Hz. A pre-load was used, with a pre-load force of 1 gf and pre-load speed of 5 mm/min. The test speed was performed at 4 mm/min. Approximately 25 specimens were tested per sample, using a 40 mm gage length. The results of diameter measurements and tensile testing can be seen in Table 4.8. The results show that increasing the steam temperature (and maintaining constant godet speeds) leads to a decrease in diameter, with wet-jet spun fiber decreasing from 18 µm to 17.3 µm and dry-jet fiber decreasing from 42.6 µm to 38 µm. This is possible because the chain molecules within the polymer are given greater mobility at higher temperatures and as a

result, are more likely to change position, or relax. As a result, tension that previously would have caused little change in diameter of a stiff, un-stretchable fiber is now able to stretch a relaxed fiber to a smaller diameter. Also affirmed during this experiment was that decreasing diameter leads to increased tensile strength, whether the fiber is spun dry-jet or wet-jet. This is important to note, and conforms with Griffith's law of fracture [21] as discussed previously.

Table 4.8. Results of diameter and tensile strength measurements were wet-jet and dry-jet fiber

					Modulus		Stress At Break	
					GPa		MPa	
Spinnerette	Capillary (micron)	Pump (rpm)	Steam (°C)	Diameter (micron)	Avg.	Stdev	Avg.	Stdev
Wet-jet	60	5	107	18	9.72	1.06	287.00	17.00
Wet-jet	60	5	212	17.3	9.59	1.02	303.04	30.34
Dry-jet	150	31.25	110	42.6	6.21	2.08	183.86	13.10
Dry-jet	150	31.25	220	38	4.91	0.76	195.10	25.29

As noted earlier, one of the large differences between the wet-jet and dry-jet spun fibers is their diameter. When spun with the same exit velocity through each of the spinnerette capillaries, and same stretch ratios, it would be expected that the resultant fiber would have the same diameter and properties. However, the dry-jet spun fibers are much larger. This is most likely is due to the die swell that occurs during spinning. As the viscoelastic fluid flows through the capillary, elastic deformation and orientation of molecules occurs. However, at the exit of the capillary, the elastic deformation accumulated through the length of the capillary relaxes, and the previously oriented material becomes disoriented, causing die swell [38]. Die swell is known to increase with the length of the capillary [38]. Therefore, it is expected that a dry-jet spinning die, with a L/D ratio of 10:1, or 1500 µm for a 150 µm capillary diameter, would have a larger die swell compared to the wet-spinning die, with a L/D ratio of 2:1, or 120 µm for a 60 µm capillary diameter. As a result, the fiber being formed during dry-jet spinning is being pulled from a much larger "pool" of fluid due to the large die swell than during wet-jet spinning, where the available

"pool" of spinning solution is essentially the same size as the diameter of the capillary plus a much smaller die swell. Also, during wet-jet spinning, when the filament exits the capillary, the relaxation of the accumulated elastic deformation is hindered slightly by the pressure of the surrounding coagulating solution. During dry-jet spinning, however, the fluid exits the capillary into air, allowing for full relaxation of the accumulated elastic deformation. Therefore, both the length of the capillary and the air gap contribute to larger die swell and therefore a larger fiber.

Dry-jet spinning can result in smaller diameter fiber when compared to wet-jet spinning, but relies on an increased spin draw. When spun at the same draw down ratios, it is easy to spot a visible difference between the spinning tensions. This is most likely due to the differences in coagulation timing. For example, wet-jet spun fibers enter the coagulating solution immediately, instantly beginning to form a skin structure. As a result of this skin formation, the fiber develops a modulus, or resistance to deformation. Any tension on the fiber is placing tension on this instantly formed skin, which resists deformation beyond a certain limit. In dry-jet spinning, however, the use of the air gap means that any tension on the fiber is applied to uncoagulated solution with a modulus close to zero, and is able to undertake large amounts of deformation before breaking and tolerate larger spin draw ratios. The maximum spin draw ratio is determined at the breakage of the fluid stream. This breakage of viscoelastic fluid jets results from excessive storage of elastic energy. It occurs once a critical stress level is reached, as seen in the following equation [39].

$$\sigma_c = \sqrt{2KE}$$

Where σ_c is the critical stress applied to the fluid jets, K and E are the cohesive energy density and tensile modulus of the fluid flow, respectively [39]. Not only does the use of the air gap lead to larger spin draw ratios, but it has also been suggested to reduce the skin-core structure and alter the fibrillar structure of the fiber, therefore leading to a stronger fiber. Scanning electron microscopy (SEM) of several wet-jet and dry-jet samples has led to a similar conclusion.

Figure 4.8 shows a SEM image taken of a 20 wt.% PAN-co-MA/DMAc sample of precursor fiber. The smooth surface structure is evident, especially when compared with Figure 4.9, an example of wet-jet spun fiber from 18 wt.% PAN-co-MA/DMAc. The use of the air gap allows the polymer fluid to form a smooth surface before entering the coagulant, whereas wet-jet spinning carries any defects resulting from the capillary, stretch, etc. directly into the resultant fiber.

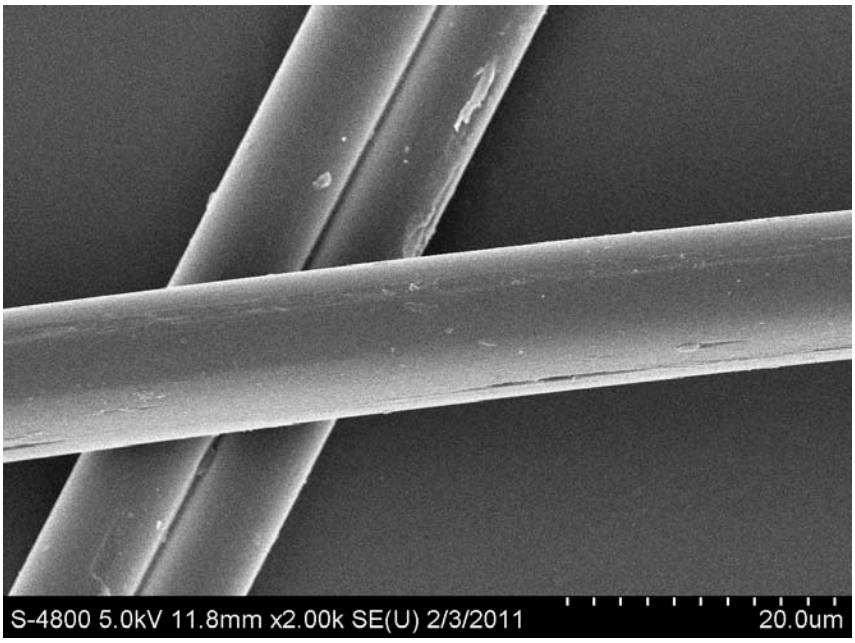

Figure 4.8. Smooth surface of dry-jet spun precursor of 20 wt.% PAN-co-MA/DMAc

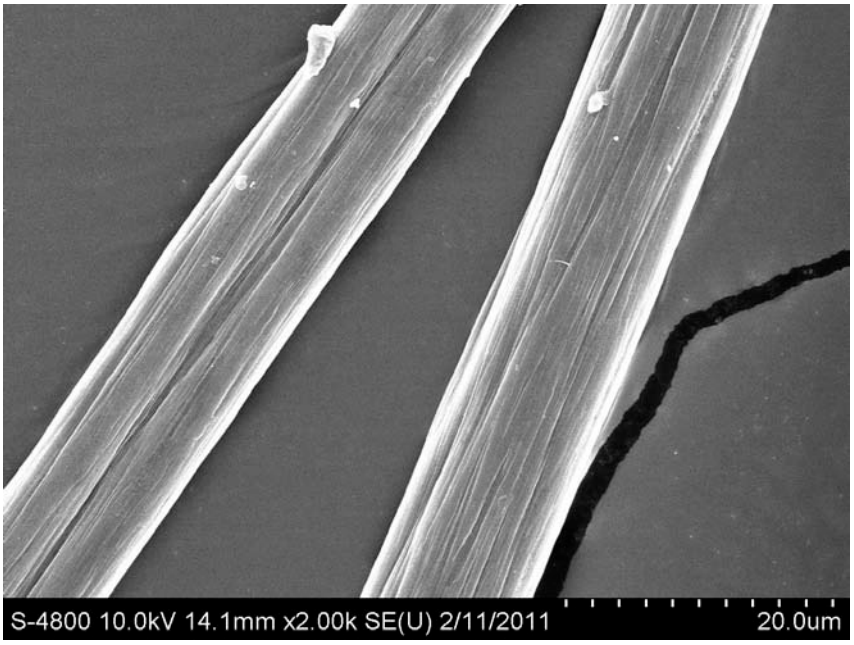

Figure 4.9. Fibrillar surface of wet-jet spun precursor fiber of 18 wt.% PAN-co-MA/DMAc

The result of these surface characteristics causes changes in the appearance of the fiber, with dry-jet spun fiber having a very high luster, seen in Figure 4.10, when compared to the low luster of wet-jet spun fiber in Figure 4.11. This is due, again, to the dry-jet fiber being pulled from a "pool" of spinning solution, allowing for the erasure of any defects that may be present in the fluid from the capillary which result in a fibrillar structure for the wet-jet samples.

Figure 4.10. High luster of dry-jet spun fiber

Figure 4.11. Low luster due to surface defects of wet-jet spun fiber

4.4 Conclusions

After analyzing the effect of spin draw, stretch, and total DDR, it was concluded that the spin draw had the most direct effect on the diameter of the resulting fiber. This was understood due to the fiber's structure beginning to be formed from the instant it enters the coagulating bath, along with the large influence on the total DDR. When comparing wet-jet and dry-jet spinning methods, it was found that when operating at the same fluid velocities, dry-jet spinning allowed for more flexibility in the spin draw speeds, with the possibility of increasing the spin draw to well above that of wet-jet spinning. It was found that despite the spinning method, diameter was the main determinant of tensile strength, consistent with Griffith's theory. Modulus is also found to increase with smaller diameter fibers, as smaller diameter fibers are often caused by high draw down ratios and therefore increased orientation. There were also marked differences in the structure of the wet-jet and dry-jet spun fiber, with the dry-jet presenting a smooth, uniform surface, due to the time given for adjustment of flaws within the air gap. The fiber produced due to wet-jet spinning continues to show a fibrillar surface, possibly leading to weaker fiber when compared to dry-jet fiber of the same diameter.

5 Final Statements

In conclusion, the results presented in this thesis have shown the effect of varying coagulation rates on fiber shape, density and porosity, the effect of fiber diameter on the tensile strength of the fiber, and has investigated the most effective method for the reduction of fiber diameter.

While some have postulated that fibers are more circular at higher bath temperatures and higher solvent contents in the coagulation baths, it was found that there is a practical limit to the high temperatures and high concentrations that can produce circular fibers. From the results, it was determined that above 8.4 °C and 60 wt.% bath concentration, fiber coagulation is slowed to the point that the fiber structure begins to degrade. Low coagulation temperatures have also been postulated to lead to a reduction in void content and increased density and fiber strength. Through experimentation, it was determined that low coagulation temperatures indeed produce a fiber with fewer voids, however, density was found to increase with increasing temperature due to the presence of residual DMAc and non-communicating voids. In order to analyze the coagulation of the fiber as it proceeds down the spinline, the residual DMAc content of the fiber was analyzed and showed a final residual content of 1.21 wt.% DMAc. This demonstrates smooth, gentle, and homogenous coagulation as the fiber moves down the line. Therefore, in order to produce a high quality precursor with circular cross section, high density, and low void content, the preferred coagulation conditions were found to be at low temperature and high concentration of solvent in the coagulation bath.

After analyzing the effect of spin draw, stretch, and total DDR, it was concluded that the spin draw had the most direct effect on the diameter of the resulting fiber. This was understood due to the fiber's structure beginning to be formed from the instant it enters the coagulating bath, along with the large influence on the total DDR. When comparing wet-jet and dry-jet spinning methods, it was found that when operating at the same fluid velocities, dry-jet spinning allowed for more flexibility in the spin draw speeds, with the possibility of increasing the spin draw to well above that of wet-jet spinning. It was found that despite the spinning method, diameter was the main determinant of tensile strength, consistent with Griffith's theory. Modulus is also found to increase with

smaller diameter fibers, as smaller diameter fibers are often caused by high draw down ratios and therefore increased orientation. There were also marked differences in the structure of the wet-jet and dry-jet spun fiber, with the dry-jet presenting a smooth, uniform surface, due to the time given for adjustment of flaws within the air gap. The fiber produced due to wet-jet spinning continues to show a fibrillar surface, possibly leading to weaker fiber when compared to dry-jet fiber of the same diameter.

In conclusion, the use of the bench-scale, multifilament spinning line in this thesis allowed for the analysis of the spinning conditions on the structure and properties of the resulting polyacrylonitrile precursor fiber. Therefore, the results presented previously show the analysis of a small, but important, number of factors on the structure and properties of the precursor fiber and allow for the production of a precursor fiber with increased tensile strength and modulus, as well as increased knowledge of fiber behavior under the discussed conditions.

REFERENCES

1. *R.B. Mathur, O.P.B., and J. Mittal, Advances in the Development of High-Performance Carbon Fibres from PAN Precursor. Composites Science and Technology, 1993.* ***51****: p. 223-230.*
2. *Juan Chen, C.W., Heyi Ge, Yujun Bai, Yanxiang Wang, Effect of Coagulation Temperature on the Properties of Poly(acrylonitrile-itaconic acd) Fibers in Wet Spinning. J. Polym. Res., 2007.* ***14****: p. 223-228.*
3. *Masson, J.C., Acrylic Fiber Technology and Applications. 1995.*
4. *Gong-qiu Peng, Y.-f.W., Yong-gang Yang, and Lang Liu, A Novel Method for Investigating the Structural Uniformity of Polyacrylonitrile Nascent Fibers. International Journal of Polymer Anal. Charact., 2008.* ***13****: p. 369-375.*
5. *M.A. Rahman, A.F.I., A. Mustafa, B.C. Ng, H. Hasbullah, M.S.A. Rahaman and M.S. Abdullah, The Effect of Coagulation Bath Temperature on the Mechanical Properties of PAN-based Carbon Fiber. p. 169-179.*
6. *Morgan, P., Carbon Fibers and Their Composites. 2005, Boca Raton: Taylor & Francis Group.*
7. *S.J. Law, S.K.M., Investigation of Wet-Spun Acrylic Fiber Morphology by Membrane Technology Techniques. Journal of Applied Polymer Science, 1996.*
8. *A.K. Gupta, D.K.P., Pushpa Bajaj, Acrylic Precursors for Carbon Fibers. Journal of Macromolecular Science, 1991.* ***C31****(1): p. 1-89.*
9. *Lewin, M., Handbook of Fiber Chemistry. 2007.*
10. *Jin-Shy Tsai, W.-C.S., Control of Cross-Section Shape for Polyacrylonitrile Fibre During Wet-Spinning. Journal of Materials Science Letters, 1991.* ***10****: p. 1253-1256.*
11. *Juan Chen, C.-g.W., Xing-guang Dong, and Huan-zhang Liu, Study on the Coagulation Mechanism of Wet-Spinning PAN Fibers. Journal of Polymer Research, 2006.* ***13****: p. 515-519.*
12. *Knudsen, J., The Influence of Coagulation Variables on the Structure and Physical Properties of an Acrylic Fiber. Textile Research Journal, 1963.* ***33****(13).*
13. *Sea Cheon Oh, Y.S.W., and Yeong-Koo Yeo, Modeling and Simulation of the Coagulation Process of Poly(acrylonitrile) Wet-Spinning. Industry and Engineering Chemistry Research, 1996.* ***35****: p. 4796-4800.*
14. *Norr, F.R.B.a.M.K., A Three-Dimensional Structural Model for a High Modulus Pan-Based Carbon Fibre. Composites, 1976.*
15. *J.P. Craig, J.P.K.a.V.F.H., Characterization of Acrylic Fiber Structure. Textile Research Journal, 1962.* ***32****(435).*
16. *Dumbleton, J.P.B.a.J.H., Changes in the Structure of Wet-Spun Acrylic Fibers During Processing. Textile Research Journal, 1971.* ***41****: p. 196-203.*

17. *Heyi Ge, H.L., Juan Chen, Chengguo Wang, The Skin-Core Structure of Poly(acrylonitrile-itaconic acid) Precursor Fibers in Wet-Spinning. Journal of Applied Polymer Science, 2007.*
18. *Moreton, R., Spinning of Polyacrylonitrile Precursor Fibres with Reference to the Properties of Carbon Fibres. Conference on Industrial Carbons and Graphite, 1971.*
19. *J.P. Craig, J.P.K., and V.F. Holland, Characterization of Acrylic Fiber Structure. Textile Research Journal, 1962.* ***32****(6): p. 435-448.*
20. *Thorne, D.J., Distribution of Internal Flaws in Acrylic Fibers. Journal of Applied Polymer Science, 1970.* ***14****: p. 103-113.*
21. *Griffith, A.A., The Phenomena of Rupture and Flow in Solids. Philosophical Transactions of the Royal Society of London, Series A, 1921.* ***221****: p. 163-198.*
22. *Christopher J.S. Petrie, A.P., Spinning Viscosity. Journal of Non-Newtonian Fluid Mechanics, 1995.* ***57****: p. 83-101.*
23. *J. Ferguson, C.D., G.R. McKay, Rheological and Coagulation Features in the Wet Spinning Process. Journal of Non-Newtonian Fluid Mechanics, 1980.* ***6****: p. 333-338.*
24. *Gareth H. McKinley, O.B., Minwu Yao, Filament Stretching Rhoemetry and the Extensional Viscosity of Dilue and Concentrated Polymer Solutions. Proc. 1st International Symposium on Applied Rheology, 2001.*
25. *T. Sridhar, V.T., D.A. Nguyen, and R.K. Gupta, Measurement of Extensional Viscosity of Polymer Solutions. Journal of Non-Newtonian Fluid Mechanics, 1991.* ***40****: p. 271-280.*
26. *Han, C.D., A Theoretical Study on Fiber Spinnability. Rheologica Acta, 1969.*
27. *Terrill, H.O.a.E.L., A Mathematical Model for the Wet-Spinning Process. European Journal of Applied Mathematics, 1992.* ***4****: p. 341-360.*
28. *Petrie, J.M.a.C.J.S., Encyclopedia of Fluid Mechanics.* ***6****: p. 112-139.*
29. *Gupta, R.K., Polymer and Composite Rheology. 2nd ed. 2000, New York: Marcel Dekker, Inc. .*
30. *Katz, J., Introductory Fluid Mechanics. 2010, New York: Cambridge University Press.*
31. *Thermo Scientific HAAKE CaBER 1.*
32. *Jin-Shy Tsai, W.-C.S., Control of Cross-Section Shape for Polyacrylonitrile Fibre During Wet-Spinning. Journal of Material Science Letters, 1991.* ***10****: p. 1253-1256.*
33. *Xing-guang Dong, C.-g.W.a.C.J., Study on the Coagulation Process of Polyacrylonitrile Nascent Fibers during Wet-Spinning. Polymer Bulletin, 2006.* ***58****: p. 1005-1012.*
34. *Mukhopadhyay, S.J.L.a.S.K., Investigation of Wet-Spun Acrylic Fiber Morphology by Membrane Technology Techniques. Journal of Applied Polymer Science, 1996.* ***62****: p. 32-47.*
35. *Skau, E.L., Simple Expressions for the Circularity and Fullness of Fibers. Textile Research Journal, 1951.* ***21****: p. 14-17.*

36. *B'Hymer, C., Residual Solvent Testing: A Review of Gas-Chromatographic and Alternative Techniques. Pharmaceutical Research, 2003.* ***20****(3).*
37. *Simon, V., Analysis of Fiber Formation during Air-Gap Wet Spinning. AIChE Journal, 1995.* ***41****(5): p. 1281-1294.*
38. *Lobanova, E.A.P.a.G.A., The Die Swell of Concentrated Solutions of Acrylonitrile Polymers and Copolymers. Khimicheakie Volokna, 1975.* ***4****: p. 17-19.*
39. *Lianjiang Tan, H.C., Ding Pan, Ning Pan, Investigating the Spinnability in the Dry-Jet Wet Spinning of PAN Precursor Fiber. Journal of Applied Polymer Science, 2008.*

VITA

Elizabeth Ashley Morris

Born October 7, 1985, Louisville, Kentucky

Education

Bachelor of Science, Mechanical Engineering, University of Kentucky, Lexington, Kentucky, USA, August 2004-December 2009.

Graduate studies, University of Kentucky, Center for Applied Energy Research, Lexington, Kentucky, USA, April 2007-May 2011. Advisor: Dr. Rodney Andrews.

Professional positions

2010-2011	Graduate Research Assistant, Center for Applied Energy Research, University of Kentucky, Lexington, Kentucky.
2007-2009	Undergraduate Research Assistant, Center for Applied Energy Research, University of Kentucky, Lexington, Kentucky.

Awards and scholarships

2010-2011	University of Kentucky, Center for Applied Energy Research, Research Assistantship.
2004-2008	University of Kentucky, Presidential Scholarship.

Conference proceedings

Ashley Morris, Matthew C. Weisenberger, John Craddock, Keith Roberts, and Rich Foedinger. *Overview of 100 Filament Bench Scale Spinning Methods for Experimental PAN-Based Precursor Fiber*. International Carbon Conference; 2010; Clemson, South Carolina, USA; 2010.

Ashley Morris, Matthew C. Weisenberger, John Craddock, Keith Roberts, and Rich Foedinger. *Advancements in 100 Filament Bench Scale Spinning of PAN-Based Precursor Fiber*. Society for the Advancement of Material and Process Engineering; 2010; Seattle, Washington, USA; 2010.

Ashley (Whitlow) Morris, Carissa Dowden, Matthew C. Weisenberger, John Craddock, Rodney Andrews, and Keith Roberts. *Tensile Properties of PAN-based Carbon Fiber Containing Multiwall Carbon Nanotubes.* International Carbon Conference; 2009; Biarritz, France; 2009.